Science of the Total Environment 952 (2024) 175840

Contents lists available at ScienceDirect

Science of the Total Environment

journal homepage: www.elsevier.com/locate/scitotenv

Black carbon and particle lung-deposited surface area in residential wood combustion emissions: Effects of an electrostatic precipitator and photochemical aging

A. Mukherjee [a,*], A. Hartikainen [a,*], J. Joutsensaari [b], S. Basnet [a], A. Mesceriakovas [a], M. Ihalainen [a], P. Yli-Pirilä [a], J. Leskinen [a], M. Somero [a], J. Louhisalmi [a], Z. Fang [c], M. Kalberer [d], Y. Rudich [c], J. Tissari [a], H. Czech [e,f], R. Zimmermann [e,f], O. Sippula [a,g,**]

[a] Department of Environmental and Biological Science, University of Eastern Finland, Kuopio 70210, Finland
[b] Department of Technical Physics, University of Eastern Finland, Kuopio 70210, Finland
[c] Department of Earth and Planetary Science, Weizmann Institute of Science, Rehovot 7610001, Israel
[d] Department of Environmental Sciences, University of Basel, Basel, Switzerland
[e] Group of Comprehensive Molecular Analytics, Helmholtz Zentrum München, Neuherberg 85764, Germany
[f] Department of Technical and Analytical Chemistry, University of Rostock, Rostock 18056, Germany
[g] Department of Chemistry, University of Eastern Finland, Joensuu 80101, Finland

HIGHLIGHTS

- eBC and LDSA emissions correlate well in residential wood combustion emissions.
- Photochemical aging increased LDSA emissions and weakened eBC/LDSA correlation.
- Wood stove ESP reduced fine particle mass, eBC and LDSA by roughly 70 %.
- ESP strongly increased the number emissions of small nanoparticles.
- Combustion phase influences particle lung deposition fractions.

GRAPHICAL ABSTRACT

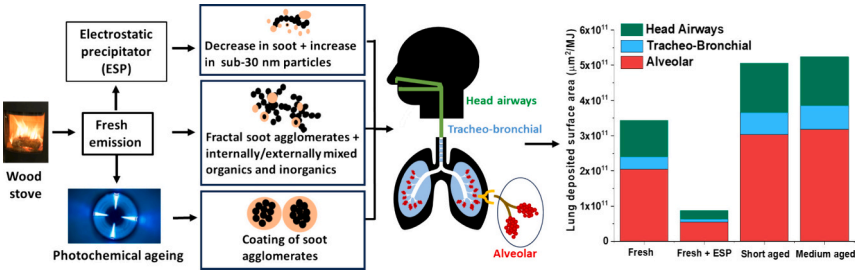

ARTICLE INFO

Editor: Hai Guo

Keywords:
Air pollution
Particulate matter
Emission factors
Biomass burning
Emission reduction
Oxidative flow reactor

ABSTRACT

Residential wood combustion (RWC) remains a significant global source of particulate matter (PM) emissions with adverse impacts on regional air quality, climate, and human health. The lung-deposited surface area (LDSA) and equivalent black carbon (eBC) concentrations have emerged as important metrics to assess particulate pollution. In this study we estimated combustion phase-dependent emission factors of LDSA for alveolar, tracheobronchial, and head-airway regions of human lungs and explored the relationships between eBC and LDSA in fresh and photochemically aged RWC emissions. Photochemical aging was simulated in an oxidative flow reactor at OH• exposures equivalent to 1.4 or 3.4 days in the atmosphere. Further, the efficiency of a small-scale electrostatic precipitator (ESP) for reducing LDSA and eBC from the wood stove was determined. For fresh emission eBC correlated extremely well with LDSA, but the correlation decreased after aging. Soot-dominated flaming phase showed the highest eBC dependency of LDSA whereas for ignition and char burning phases

* Corresponding authors.
** Corresponding author at: Department of Environmental and Biological Science, University of Eastern Finland, Kuopio 70210, Finland.
E-mail addresses: arya.mukherjee@uef.fi (A. Mukherjee), anni.hartikainen@uef.fi (A. Hartikainen), olli.sippula@uef.fi (O. Sippula).

https://doi.org/10.1016/j.scitotenv.2024.175840
Received 10 May 2024; Received in revised form 14 August 2024; Accepted 26 August 2024
Available online 28 August 2024

non-BC particles contributed strongly the LDSA. Deposition to the alveolar region contributed around 60 % of the total lung-deposition. The ESP was found as an effective method to mitigate particulate mass, LDSA, as well as eBC emissions from wood stoves, as they were reduced on average by 72%, 71%, and 69%, respectively. The reduction efficiencies, however, consistently dropped over the span of an experiment, especially for eBC. Further, the ESP was found to increase the sub-30 nm ultrafine particle number emissions, with implications for LDSA. The results of this study can be used for assessing the contribution of RWC to LDSA concentrations in ambient air.

1. Introduction

Particulate emissions from global traffic and industries have decreased continuously over the years due to stricter emission regulations, but the level of residential scale wood combustion (RWC) emissions has remained stable or, in many cases, steadily increased (Savolahti et al., 2019a; Chen et al., 2017; Kukkonen et al., 2020). RWC emissions have been found to dominate urban air particle pollution in several European cities, and have been estimated to cause severe climate, air quality, and health impacts (Kaskaoutis et al., 2022; Lelieveld et al., 2015; Janssen et al., 2011; Moreno-Ríos et al., 2022; Savolahti et al., 2019b; IPCC, 2014). When inhaled, RWC exhaust particles may, for example, induce formation of reactive oxygen species (ROS) and cause adverse pulmonary, cardiovascular, and carcinogenic effects (Moreno-Ríos et al., 2022). Particles from batch-wise logwood combustion are typically dominated by soot formed in the flame and exhibit fractal agglomerate structures composed of small elemental carbon (EC) spherules and complex mixtures of organic matter (Kortelainen et al., 2018; Michelsen et al., 2020). The main carbonaceous and highly light absorbing part of soot is routinely measured as equivalent black carbon (eBC) in several ambient sites across the world (Ni et al., 2014; Helin et al., 2018). Part of the fine particulate matter is also formed by ash released from fuel, the predominant compounds being potassium and sodium sulfates, chlorides, carbonates and zinc oxide (e.g., Chen et al., 2017; Czech et al., 2018; Kortelainen et al., 2018; Lamberg et al., 2018; Sippula et al., 2007). Further, organic matter can be either internally or externally mixed with soot and ash particles. In the first case, organic coating is typically formed around soot or ash particles via condensation of initially released organic vapours during the flue gas cooling (Tissari et al., 2008; Torvela et al., 2014). In the second case, particles may be formed entirely of organic matter (Chakrabarty et al., 2006; Torvela et al., 2014). Particle transformation also continues in the atmosphere due to, for example, coagulation and formation of secondary organic aerosol (SOA) via oxidation of organic precursor gases emitted from RWC (Bruns et al., 2015; Tiitta et al., 2016; Bertrand et al., 2017).

The surface area of particles deposited in the human respiratory tract has been proposed as potential metric to assess health effects of ambient fine particulate matter, as the particle toxicity seems to correlate with the nanoparticle surface area, which can be explained by the surface interactions of the non-soluble particles with respiratory track membranes (Oberdörster et al., 2005; Löndahl et al., 2009; Schmid and Stoeger, 2016; Nicolaou et al., 2021). For northern European modern wood stoves, the non-soluble particles are mostly composed of EC (Basnet et al., 2024; Kortelainen et al., 2018). Concerning lung toxicity, the major particle deposition regions can be divided into the upper respiratory tract or head airways (HA), tracheobronchial (TB), and alveolar (ALV) regions (Guarnieri and Balmes, 2014; Koullapis et al., 2020; Vicente et al., 2021). The lung-deposited surface areas (LDSA) at different parts of the human respiratory tract can be estimated by measurements of the particle size distributions, and by using a model predicting the size-dependent deposition efficiencies of particles in the human respiratory tract (ICRP, 1994). However, unlike traditional metrics for particulate emissions such as particulate mass ($PM_{2.5}$ or PM_{10}), LDSA concentrations remain largely unregulated (WHO, 2021). This is due to lack of widespread standardised measurements, as well as the scarcity of studies combining estimates of LDSA with toxicological or epidemiological findings (Liu et al., 2023).

In ambient air of major cities, the LDSA concentrations tend to be at their peak near the particle size of 100 nm (Fierz et al., 2011; Reche et al., 2015; Kuuluvainen et al., 2016; Hama et al., 2017; Kuula et al., 2020; Cheristanidis et al., 2020), which concurs with the typical size range of black carbon particles (Kumar et al., 2010; Grahame et al., 2014). eBC and LDSA concentrations have been shown to correlate in traffic emissions (Hama et al., 2017; Cheristanidis et al., 2020; Kuula et al., 2020; Liu et al., 2023), in harbour environment (Lepistö et al., 2022), and in wood combustion emissions in residential areas (Kuula et al., 2020). These findings emphasize the importance of black carbon containing particles towards lung toxicity, especially as they may serve as carriers of toxic materials into the lung alveoli (so-called Trojan horse effect) (Ortega et al., 2014). Despite the observed correlations between eBC and LDSA in ambient air, the connection between eBC and the lung-deposition of particles has not been established for RWC, and the effects of combustion conditions on this connection are not known. Further, atmospheric transformation likely influences the LDSA of RWC-derived aerosols due to secondary aerosol formation and morphological changes of primary particles, including particle growth and compaction (Leskinen et al., 2023; Corbin et al., 2023). Changes in particle size and density may influence deposition efficiencies and alter both the correlation of LDSA and eBC and the potential toxicity of RWC emissions in the lungs.

Currently, European regulations are implemented partly within the European Ecodesign Directive (Directive 2009/125/EC), national air pollution acts, and via voluntary "Ecolabels" of woodstoves (e.g., German Blue Angel; Tebert et al., 2020). In the near future, there is an urgent need for more stringent emission regulations to RWC appliances due to the growing concerns of air pollution by residential heating. Small electrostatic precipitators (ESP) show promise for abating particulate emissions from wood stoves and several different small-scale ESPs have recently been introduced to the market (Jaworek et al., 2021; Brunner et al., 2018). Previous studies have reported large variation in particle matter reduction efficiencies (30–98 %) by ESPs for RWC emissions, depending on the ESP operating conditions and the used measurement methods and metrics (Brunner et al., 2018; Cornette et al., 2024). In addition, long-term usage may considerably impair the reduction efficiencies of ESPs (Oehler and Hartmann, 2014). Due to the ESP's particle size dependent charging efficiencies, combustion phase dependent reduction efficiencies, potential promotion of ultrafine particle formation by nucleation and re-entrainment of collected particles to the flue gas flow, the ESPs also considerably change size distributions of the emitted particles (Suhonen et al., 2021; Omara et al., 2010; Cornette et al., 2024), which would also influence LDSA in the exhaust. To our knowledge, the efficiency of small wood stove ESPs towards LDSA reduction has not been studied previously.

The objective of this work was to estimate the emission factors of particulate LDSA from RWC during the different phases of residential wood combustion in fresh and photochemically aged exhausts. The connection between the LDSA and eBC emissions over the ignition, flaming, and residual char burning phases was studied in order to evaluate the role of RWC-derived eBC emissions for ambient air LDSA concentrations. Further, the particle morphologies and the size-dependent effective densities of fresh and photochemically aged particles from the different combustion phases were assessed with the aim of understanding the impact of atmospheric transformation and restructuring of particulate emissions to LDSA. Finally, the eBC and LDSA

reduction efficiencies of an ESP were determined and the impact of an ESP on the relationship of LDSA and eBC emissions from RWC established. The results help to evaluate the efficiency of ESP as a mitigation method to decrease the BC and LDSA emissions from RWC to ambient air.

2. Material and methods

2.1. Experimental setup

The experiments were conducted in the ILMARI research facility at University of Eastern Finland. A modern chimney stove (Aduro 9.3, Aduro A/S) equipped with combustion air staging system was fired with beech logwood. The composition of the beech wood is shown in Supplementary Table S1. Each 4 h experiment consisted of in total six consecutive batches of 2 kg logwood, each burning for 35 min, and a residual char-burning phase for the final 30 min. For studying the impact of an ESP on the particulate emissions, an OekoTube (Oekosolve) 'electrostatic precipitator inside' -unit was installed in the flue gas stack. This device is a tube-type ESP specifically designed for small-scale wood combustion appliances and represents a typical small-scale ESP technology commercially available in European market. In it, the particles are electrically charged and separated from the flue gas flow by electrostatic forces (Brunner et al., 2018). The metallic inner wall of the chimney is used as the ground electrode to which the particles are deposited. The wood stove was operated either with ESP off or on throughout the 4-h fresh experiments, and the removal efficiencies were determined by comparing the average emission factors in fresh emissions from experiments with the ESP turned on with those recorded with the ESP off. Furthermore, the effect of atmospheric processing, i.e., 'aging', on the wood combustion emissions were investigated using an oxidation flow reactor as described in Section 2.2. A total of 12 individual experiments were carried out with 3 replicates for each type of experiment (fresh emissions with ESP off and ESP on, and aged emissions with two different aging settings).

The flue gas was sampled through a pre-cut PM_{10} cyclone and a heated (180 °C) tube into a two-stage diluter consisting of a porous tube diluter and an ejector diluter (*DAS*, Venacontra). A dilution of 1:60 was performed on the flue gas before passing it either through the Photochemical Emission Aging flow tube Reactor (PEAR; Section 2.3) to measure aged emissions, or a bypass tube to measure fresh emissions. Dilution in the porous tube dilutor was very stable throughout the experiments, with a temporal variation in the range of 0.2–0.3 %. Dilution of the aged emissions was 1:65 due to the internal dilution in the PEAR by H_2O and O_3. Samples were additionally diluted by ejector dilutors (Palas) before the particle phase instrumentation. The degree of dilution was defined from CO_2 concentrations in the raw gas, in the diluted sample, and after the PEAR. A schematic view of the experimental setup is available in the Supporting Information (Fig. 1).

2.2. Gas phase measurements

A multicomponent Fourier Transform Infrared Spectrometer (FTIR, *DX4000*, Gasmet Technologies Oy) was incorporated to the stack to characterize the fresh exhaust gases in all 12 experiments. The FTIR measurements included online monitoring of, e.g., O_2, CO_2, CO, NO, NO_2, CH_4, and 30 non-methane volatile organic compounds (NMVOCs) typical for combustion emissions. NMVOCs were further grouped into aliphatic hydrocarbons, aromatic compounds, and non-aromatic oxygenated compounds (Supplementary Table S2). CO_2 concentrations in the fresh exhaust, diluted sample, and after the PEAR were monitored by nondispersive infrared CO_2 monitors (*ULTRMAT 23*; Siemens, *AO2040*; ABB and *GMP343*; Vaisala respectively).

2.3. Photochemical Emission Aging flow tube Reactor (PEAR)

Photochemical aging of the exhaust aerosol sample was carried out using the Photochemical Emission Aging flow tube Reactor (PEAR; Ihalainen et al., 2019). The PEAR has a volume of 139 l and it was operated at a total flow rate of 130 l per minute (lpm)resulting in an average residence time of 64 s. In the PEAR, UV lights, centred at 254 nm, photolyze the externally fed O_3, leading to extensive production of hydroxyl (OH•) radicals and consequently rapid photochemical processing of the aerosol sample. Relative humidity in the PEAR varied slightly depending on the flue gas moisture and was 54 % ± 5 % over all the experimental time. Temperature in the PEAR was 23.8 ± 1.0 °C. The input concentration of O_3 was 9 ppm. Two different lamp settings were utilized to generate either "short aged" or "medium aged" conditions with respect to the maximum PM atmospheric lifetime of approximately two weeks. OH• exposure was determined using d9-butanol as an external 'OH clock' (Barmet et al., 2012). d9-butanol was fed to the PEAR alongside the sample throughout the combustion experiments at a rate of 0.008 lpm, and the concentration downstream the PEAR was monitored with a proton-transfer reaction time-of-flight mass

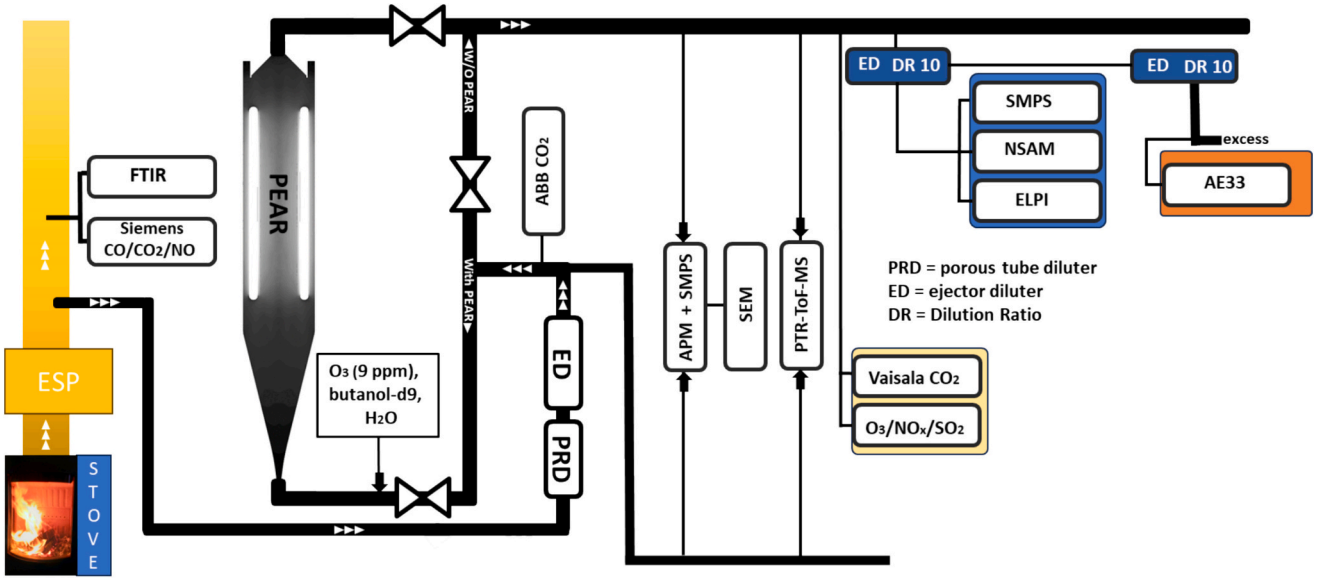

Fig. 1. A schematic diagram of the experimental setup.

spectrometer (PTR-ToF 8000, Ionicon). The short and long conditions were estimated to correspond to 1.4 ± 0.3 or 3.4 ± 0.4 equivalent photochemical days of aging, respectively, assuming ambient OH concentration of 1.5×10^6 cm^{-3} (Supplementary Fig. S1a-b).

The external OH• reactivity in the sample (OHR_{ext}) was retained by dilution of the exhaust gases. OHR_{ext} in the PEAR was estimated based on the gaseous components measured by the Fourier Transform Infrared Spectrometer (FTIR, *DX4000*, Gasmet Technologies Oy, Supplementary Table S2) similarly to previous work (Hartikainen et al., 2020) and was on average 670 s^{-1} over the duration of the aging experiments. Due to the natural variance in the flue gas contents, aging also varied during the experiments, with the highest OH• exposures achieved during the residual char burning phase when the OHR_{ext} was the lowest (Supplementary Fig. S1c-d). The reaction pathways in the PEAR may deviate from those in the atmosphere, for example due to the rapid processing not allowing for isomerization of formed peroxyl radicals, while UVC photolysis is more pronounced than in the troposphere (e.g., Peng and Jimenez, 2020). However, the exposure conditions remained generally relevant of tropospheric conditions, with average photolysis/OH• exposure-ratios of 2.6×10^6 and 1.7×10^6 cm $second^{-1}$ for short and medium aging experiments, respectively (Supplementary Fig. S1e-f).

2.4. Measurements of particle morphology, size, and mass

The particle effective densities (ρ_{eff}) and mass mobility exponents (D_{fm}), describing the size-dependency of ρ_{eff}, were measured using an Aerosol Particle Mass Analyzer (*APM 3602*, Kanomax Inc.) coupled with a Scanning Mobility Particle Sizer (SMPS, with *CPC 3776* and *DMA 3081*, TSI Inc.), similarly to Leskinen et al., 2023. Details of the methodology can be found in the supplemental material (Supp. Section S1). The APM-SMPS measurements were performed separately for each of the three combustion phases using a stabilizing chamber. The specific sampling periods for the APM-SMPS measurements are available in Supplementary Table S3. Mean effective densities were calculated for each combustion phase by weighting the size-resolved ρ_{eff} by the particle number size distributions measured from the stabilizing chamber by the SMPS without the APM (Charvet et al., 2015). In addition, particles were collected from the APM-SMPS stabilizing chamber on holey carbon grids (S147–4 Holey carbon film 400 Mesh Cu, Agar Scientific Inc.) for electron microscopy. The sampling was performed through an aspiration sampler at a flowrate of 0.3 lpm. The particle morphologies of the non-aged and aged particles from the different combustion phases were then viewed with a scanning electron microscope (SEM, Sigma HD/VP, Carl Zeiss NTS).

Particle size distributions in the diluted exhaust were continuously monitored by an additional SMPS (with *DMA 3081* and *CPC 3750*, TSI Inc.) and an Electrical Low Pressure Impactor (*Classic ELPI*, Dekati Ltd.) with sintered impactor plates and the filter stage in use. For the ELPI, the eight lowest size bins were utilized for determining the particle number (N_{ELPI}), mass ($PM_{0.9}$), and surface area of particles below the size of 0.9 μm in aerodynamic diameter. The submicron particle mass ($PM_{0.9}$) was estimated from the particle number values using the particle-size dependent effective densities measured for the different combustion phases.

Equivalent (e)BC was measured by a dual-spot aethalometer (*AE33*, Magee Scientific), which measures the light attenuation at seven wavelengths (Drinovec et al., 2015). The absorption coefficient at 880 nm was converted to eBC mass using the standard mass absorption cross-section of 7.77 m^2 g^{-1} at 880 nm. Multiple scattering coefficient (C) of 1.39 was applied as recommended by the filter manufacturer for the PTFE/PET-coated glass fiber filter tape (M8060) in use. C depends on the optical properties of the sampled exhaust particles, and differences with the actual and applied C would cause proportional changes in the absolute black carbon concentrations (Yus-Díez et al., 2021). ELPI and SMPS measurements were carried out at a dilution of 1:600 (1650 for aged emissions), whereas an additional ten-fold dilution (in total 1:6000 for fresh, 1:6500 for aged emissions) was applied for the aethalometer.

2.5. LDSA determination

The surface area of lung-deposited particles was determined using two different online methods. Firstly, the tracheobronchial LDSA concentration was measured from the fresh or aged exhaust using the Nanoparticle Surface Area Monitor (NSAM, model *3550*, TSI) at the dilution of 1:600. NSAM charges the particles by a unipolar diffusion charger, which is followed by an adjustable ion trap to remove particles that have electrical mobility above the selected threshold (Shin et al., 2007). The total current of the particles passing through the ion trap are then measured by an electrometer and converted to the LDSA concentration using a single conversion factor, which is calibrated by the instrument manufacturer. The NSAM has been suggested to be reasonably accurate up to particle sizes of 400 nm, while the LDSA of larger particles may be underestimated (Asbach et al., 2009; Lepistö et al., 2020). NSAM can be set to measure the particle LDSA concentrations either in the alveolar (ALV) or the tracheobronchial (TB) regions of human lungs by pre-defining the ion trap voltage. Here, the tracheobronchial LDSA concentrations were measured over the whole duration of the combustion (4 h) in 10 s time resolution. The instrument default conversion factor of 80 ($\mu m^2/cm^3$)/pA was used.

Secondly, the size resolved submicron LDSA concentrations in all three major regions of the human respiratory tract, namely the ALV, TB, and HA, were assessed based on the data from the ELPI, which measured the number size distributions of emitted particles with high temporal resolution (10 s) across the entire experiment durations. Both NSAM and ELPI utilize similar unipolar charging of aerosols, after which the charge carried by the particles are measured by using electrometers. The major differences between NSAM and ELPI are that ELPI measures particle charges for several different particle size channels, whereas NSAM measures particle size fraction adjusted by a pre-defined trap voltage prior to the electrometer. We used the eight lowest size bins of the ELPI to account for submicron ($PM_{0.9}$) LDSA. The particle number weighted average effective Fig. 2 for each combustion phase were applied for the conversion of the aerodynamic size distributions measured by ELPI to mobility size distributions for particles below 500 nm in mobility diameter, which were then used for estimation of the particle surface areas for each individual size bin. For particles larger than 500 nm, the aerodynamic size distributions were used for the LDSA calculation, as

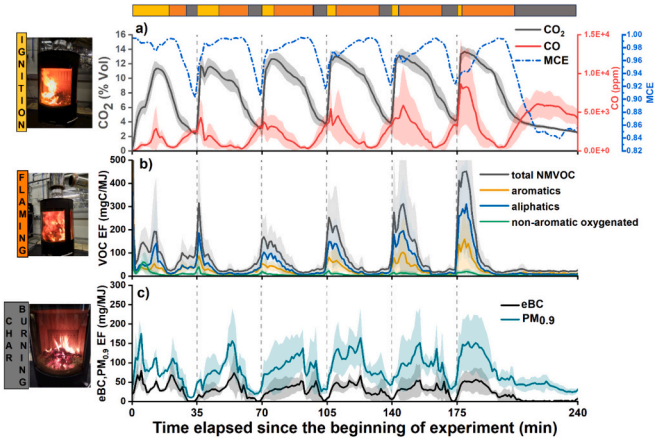

Fig. 2. Characteristics of the fresh RWC emissions: concentrations of CO_2 and CO, and MCE (a), emission factors of volatile organic compounds measured by FTIR (b), and emission factors of eBC and $PM_{0.9}$ (c). The solid lines represent the average concentration at each timepoint over all experiment days, while the shaded areas represent the standard deviations. The vertical dotted lines denote the addition of a new batch. The colorbar at the top denotes the average periods for the three combustion phases, namely ignition (yellow), flaming (orange), and char burning (grey), exemplary images of which are shown on the left.

suggested by Hinds (1999). The lung-deposition efficiency of a particle depends highly on the particle size and the region of the human respiratory system in question. The particle deposition curves modelled by the International Commission for Radioactive Protection (ICRP) were used for determining the particle LDSA concentration for the different regions of the human respiratory track based on the ELPI results (Hinds, 1999; Lepistö et al., 2020). These models represent the average deposition efficiencies for male and female respiratory tracks at three different exercise levels (sitting, light exercise, and heavy exercise) for spherical particles with constant density across the size range (Hinds, 1999). Exemplary deposition efficiency curves are shown in Supplementary Fig. S2 for densities 1 and 2 g/cc.

2.6. Data management

Each batch of combustion was divided into three phases: ignition, flaming, and residual char burning. The ignition phase was determined to last from the beginning of the batch to the moment of batch maximum flue gas CO_2 concentration, while the residual char burning phase began from the moment when the CO concentration started to elevate and remained at an elevated level until the end of the batch (Fig. 2a). In addition, modified combustion efficiency (MCE) was calculated as a simple indicator for the efficiency of the combustion process by Eq. (1):

$$MCE = \frac{CO_2}{CO_2 + CO} \quad (1)$$

where CO_2 and CO are the flue gas carbon dioxide and carbon monoxide concentrations measured by FTIR (Stockwell et al., 2014; Yokelson et al., 1997).

The emission factors (EF) of the emitted components were determined as in Reda et al., 2015. In short, the measured emission contents were corrected for the dilution, the air-fuel equivalence ratio (λ, Eq. (2)), and the flue gas moisture content. The air-fuel equivalence ratio (λ) is defined as:

$$\lambda = \frac{CO_{2\_s}}{CO_{2\_m}} \quad (2)$$

where CO_{2_s} is the carbon dioxide concentration in stoichiometric combustion of the beech logs (20.2 vol%) and CO_{2_m} is the dry carbon dioxide concentration measured from flue gas. The dry fuel net calorific value (NCV) was determined as 18.42 MJ/kg using a bomb calorimeter (European Standard ISO 18125:2017). The calculated EFs are presented as emission quantity per fuel embodied energy (#/MJ). Averaged values are presented as arithmetic means ± standard deviation during the whole experimental period.

3. Results and discussion

3.1. Combustion conditions

In general, the obtained combustion conditions can be considered good for a batch-wise wood combustion appliance, with average MCE of 0.97 ± 0.02 over the full 35 min batches when excluding the residual char burning at the end of experiments. The average MCE values were 0.98 ± 0.01 for the flaming combustion and 0.86 ± 0.05 for residual char burning. The cold start of the first wood batch of each experiment led to long ignition periods (15.6 ± 2.4 min) compared to the later batches, for which the ignition periods lasted only for 4.3 ± 2.9 min (Fig. 2). 'Smouldering' combustion with MCE below approximately 0.9 occurred only for the residential char burning phase of the last batch, which was allowed to burn out without addition of new logs. The average concentration of CO gradually increased along the 6 batches of combustion (Fig. 2a), with average EFs starting from 102 g/MJ for first batch to 596 g/MJ for the last batch. EF of NMVOCs averaged over total duration of all experiments was 4.2 ± 4.4 gC/MJ of fuel, with 34.4 % and 56.5 % contribution from the aromatic and aliphatic hydrocarbons measured by FTIR, respectively. The time resolved EFs for total NMVOCs, and the classified VOC groups measured by FTIR are shown in Fig. 2b. The majority of the NMVOC were released during the first few minutes after the ignition of a new batch, in agreement with previous studies on RWC emissions (Hartikainen et al., 2020; Kortelainen et al., 2018; Miersch et al., 2019). Mean concentrations of CO, MCE, and NMVOC EFs from the 4 h combustion procedure were also comparable to available literature data of conventional modern European wood stoves with a combustion air staging system (Czech et al., 2016; Hartikainen et al., 2020; Klauser et al., 2018).

The mean $PM_{0.9}$ emissions of the total combustion experiments were 79.5 ± 55.8 mg/MJ (approximately 120 mg/m^3 normalized to 13 % flue gas oxygen) (Table 1, Fig. 2c). These emissions are similar or somewhat higher than emissions of modern wood stoves reported in our previous studies with beech and spruce (Hartikainen et al., 2020; Ihantola et al., 2020; Suhonen et al., 2021), but clearly above the emission limits enforced for the total PM of logwood-fired stoves in the Ecodesign Directive (40 mg/m^3; European Commission, 2009). However, the emission values obtained in this study represent mostly real-world emissions of the stove, rather than standard emission test measurements. On average, the ratio of eBC to the total $PM_{0.9}$ in the fresh emissions was 0.35 ± 0.15, 0.36 ± 0.1, 0.15 ± 0.08 for ignition, flaming, and char burning phases, respectively, which generally fall into the range of studied eBC fractions in modern wood stove particulate emissions (Alves et al., 2011; Gonçalves et al., 2012).

3.2. Particle size distributions, effective density, and morphology

In the beginning of the ignition phase, the majority of the particles in the fresh emission were below 100 nm in mobility size, but quickly grew to above 100 nm when reaching flaming conditions. Finally, for the residual char burning dominated combustion, the size distribution was again dominated by small particles, with geometric mean diameter (GMD) of 48.8 ± 16.3 nm averaged over all experiment days (Table 1). The average particle mobility size distributions for different combustion phases are illustrated in Fig. 3. Time-resolved particle number size distributions measured by SMPS and ELPI are illustrated in Supplementary Figs. S3 and S4, respectively.

The effective density of fresh particles decreased with increasing particle diameter in the ignition and flaming phases (Supplementary Fig. S5a), consistent with previous assessments of RWC particle morphology (Leskinen et al., 2014, 2023). This size dependency of effective density is attributed to the fractal-like chain structures of the soot agglomerates, as also observed by electron microscopy (Supplementary Fig. S6). Further, there may be differences in the chemical compositions, as char burning phase mainly generates alkali salt particles with closed morphology, whereas the particles in other phases are dominated by soot and organics (Kortelainen et al., 2018; Leskinen et al., 2014). The mass mobility exponents of the fresh particles emitted from ignition and flaming phases were 2.5–2.7, which is corresponding to previous assessments of fresh soot agglomerates from RWC and other combustion sources (Leskinen et al., 2014; Olfert and Rogak, 2019; Pokhrel et al., 2021; Rissler et al., 2013; Wu et al., 2019). For the char burning phase, there was no mass dependency in effective densities, indicating spherical particle morphology. The effective density also varied for the different combustion conditions, with ignition, flaming and residual char burning phases having mean densities of 0.7 g/cm^3, 0.91 g/cm^3 and 2.1 g/cm^3, respectively (Table 1). The relatively higher density measured for the char burning phase are likely caused by the spherical morphology of particles and a high fraction of alkali salts in them, as concluded by Leskinen et al. (2014).

Photochemical aging led to the momentary formation of a distinct nucleation mode in the particle size distribution, centred at 45 nm, while the primary particle mode was centred at 120 nm (Supplementary Fig. S3). Nucleation of condensable vapours occurs frequently during

Table 1
Average particle emission factors and properties (mean ± std. dev) in fresh and aged RWC emissions for the three combustion phases. Particle number emission factors were measured by SMPS (N_{SMPS}) and ELPI (N_{ELPI}), mass of particles with aerodynamic diameter below 0.9 μm (PM0.9) by the ELPI, mass of eBC by aethalometer, and geometric mean mobility diameter (GMD) by SMPS. The particle number -weighted mean effective density (ρ_{eff}) and mass mobility exponent (D_{fm}) were calculated based on the APM-SMPS. The ratios of LDSA measured by NSAM or modelled based on the ELPI results to $PM_{0.9}$ are shown for the different regions of the human respiratory track.

Combustion phase	Setting	N_{SMPS} ($\times 10^{13}$ /MJ)	N_{ELPI} ($\times 10^{13}$ /MJ)	GMD (nm)	ρ_{eff} (g/cm^3)	D_{fm}	$PM_{0.9}$ (mg/MJ)	eBC (mg/MJ)	LDSA/$PM_{0.9}$ ($\times 10^9$ μm^2/mg)			
									NSAM TB	ELPI-ICRP TB	ELPI-ICRP ALV	ELPI-ICRP HA
Ignition	Fresh	2.26 ± 1.20	4.55 ± 2.03	94.2 ± 38.5	0.7	2.7	80.9 ± 48.9	28.8 ± 24.6	0.22 ± 0.06	0.45 ± 0.1	2.70 ± 0.53	1.46 ± 0.28
	Fresh + ESP	1.77 ± 2.95	2.05 ± 2.68	79.5 ± 44.3	0.7	~3	20.8 ± 23.8	5.88 ± 6.48	0.16 ± 0.20	0.44 ± 0.17	2.67 ± 0.80	1.39 ± 0.12
	Short aged	6.52 ± 10.18	6.48 ± 7.33	88.4 ± 47.4	1.2	2.9	98.3 ± 35.4	34.8 ± 34.0	0.28 ± 0.09	0.55 ± 0.22	2.93 ± 0.79	1.48 ± 0.35
	Medium aged	7.37 ± 5.49	7.12 ± 4.26	69.9 ± 41.0	1.8	~3	104 ± 43.3	55.8 ± 42.4	0.31 ± 0.11	0.77 ± 0.38	3.65 ± 1.23	1.66 ± 0.50
Flaming	Fresh	2.79 ± 0.84	5.38 ± 2.27	112 ± 33.9	0.9	2.5	102 ± 57.6	37.2 ± 26.2	0.26 ± 0.05	0.48 ± 0.12	2.87 ± 0.67	1.50 ± 0.33
	Fresh + ESP	1.52 ± 2.79	2.30 ± 3.64	81.5 ± 34.1	0.8	2.5	32.6 ± 34.4	12.1 ± 11.4	0.15 ± 0.15	0.42 ± 0.15	2.56 ± 0.63	1.30 ± 0.13
	Short aged	5.54 ± 8.10	4.69 ± 3.04	96.0 ± 46.9	1.3	2.9	113 ± 53.3	72.4 ± 50.0	0.25 ± 0.08	0.46 ± 0.15	2.58 ± 0.58	1.40 ± 0.26
	Medium aged	6.43 ± 4.44	5.40 ± 2.27	61.5 ± 35.2	1.5	~3	105 ± 38.8	64.4 ± 33.9	0.26 ± 0.06	0.60 ± 0.23	2.92 ± 0.81	1.42 ± 0.24
Residual char burning	Fresh	4.22 ± 1.41	2.71 ± 0.61	48.8 ± 16.3	2.1	a ~3	36.8 ± 18.9	5.52 ± 13.3	0.39 ± 0.13	1.00 ± 0.44	4.42 ± 1.51	1.48 ± 0.41
	Fresh + ESP	1.18 ± 2.50	0.88 ± 2.58	45.2 ± 21.7	1.1	2.5	4.65 ± 11.5	1.13 ± 1.61	0.14 ± 0.08	0.55 ± 0.22	2.64 ± 0.82	1.30 ± 0.16
	Short aged	7.27 ± 7.17	6.04 ± 5.05	58.8 ± 17.4	2.2	~3	68.8 ± 17.6	7.59 ± 13.4	0.40 ± 0.12	0.92 ± 0.40	4.07 ± 1.27	1.40 ± 0.26
	Medium aged	8.20 ± 7.24	6.49 ± 3.55	50.3 ± 12.9	2.2	~3	63.0 ± 15.1	6.47 ± 14.0	0.44 ± 0.11	1.03 ± 0.34	4.48 ± 1.11	1.54 ± 0.25

oxidative aging of combustion emissions in both ambient air (Mylläri et al., 2019) and in oxidative flow reactor experiments (Hartikainen et al., 2020; Keller and Burtscher, 2017). However, it should be noted that the aerosol dynamics in oxidation flow reactors are not representing atmospheric conditions, due to the fast oxidation reactions and higher concentrations of particles and gases in comparison to atmosphere. The fast oxidation reactions in the oxidation flow reactors have been found to promote formation of new particles via nucleation (Ihalainen et al., 2019; Keller and Burtscher, 2017).

Photochemical processing substantially increased the effective densities of ignition and flaming combustion derived particles in both the short- and medium exposure scenarios. Effective densities of short and medium aged particles ranged from 1.2 to 2.2 g/cm^3 for different combustion phases (Table 1), while the D_{fm} ranged from 2.9 to close to 3. Thus, after aging particle effective densities no longer had significant size dependency (Supplementary Fig. S5c-d). These densities and D_{fm} values indicate a substantial compaction of the particle structures during photochemical aging, which may be caused both by coating formation and possible evaporation of organic matter during the atmospheric aging (Corbin et al., 2023). In addition to compaction of the original soot particle structure, condensation of secondary organic and inorganic vapours influence particle density (Corbin et al., 2023; Enekwizu et al., 2021; Leskinen et al., 2023). The compaction of soot particles was also captured by electron microscopy. The SEM images (Supplementary Fig. S6) illustrate the collapsing of the soot agglomerates under the organic coating.

3.3. Comparison of LDSA estimates using ELPI and NSAM

The LDSA for ALV, TB and HA regions were estimated separately for submicron particles with the ELPI-ICRP model (Lepistö et al., 2020). Additionally, the TB-LDSA was also measured directly by the NSAM, with the two TB-LDSAs (measured by NSAM and ELPI-ICRP method) correlating very well ($R^2 > 0.95$) both for primary and aged emissions (Supplementary Fig. S7). In the fresh exhaust, the NSAM-based LDSA was 63 % of the TB LDSA estimated using ELPI-ICRP method (Supplementary Fig. S7). This difference between the two methods falls in line with previous studies which have compared LDSA measured by NSAM and similar unipolar diffusion charger -based instruments to those estimated from reference instruments like CPC, SMPS, ELPI and ELPI+ (Kuuluvainen et al., 2016; Lepistö et al., 2020; Ntziachristos et al., 2007; Todea et al., 2017).

After aging, the ratio of NSAM TB-LDSA to the ELPI-ICRP based TB-LDSA decreased to 53 % and 48 % for short and medium aged exhaust, respectively (Supplementary Fig. S7). The larger difference between the two sets of results upon aging suggests that higher densities result in larger discrepancy between the methods. NSAM assumes a linear relationship between diffusion charging and LDSA and uses a constant conversion factor which is calibrated for 100 nm, the size at which the instrument shows highest sensitivity (Shin et al., 2007). It is well documented that NSAM approximated LDSA concentrations are reliable in the size range of 20–400 nm, but it overestimates the LDSA concentrations of particles larger than 400 nm and underestimates the LDSA of particles smaller than 20 nm (Asbach et al., 2012; Fissan et al., 2006; Salo et al., 2021; Todea et al., 2015). As we aim to estimate the LDSA of particles up to 900 nm of aerodynamic size in this study, we primarily focus on the ELPI-ICRP method based LDSA concentrations in the subsequent sections.

3.4. Particulate LDSA in fresh RWC emissions

The emission factors of ELPI-based LDSA for fresh RWC particles averaged over all experiments were $(2.3 \pm 1.2) \times 10^{11}$ μm^2/MJ, $(3.9 \pm 1.9) \times 10^{10}$ μm^2/MJ and $(1.1 \pm 0.8) \times 10^{11}$ μm^2/MJ for ALV, TB and HA regions, respectively. LDSA in ALV covered about 60 % of the total deposited surface area, when averaged over all 6 combustion batches.

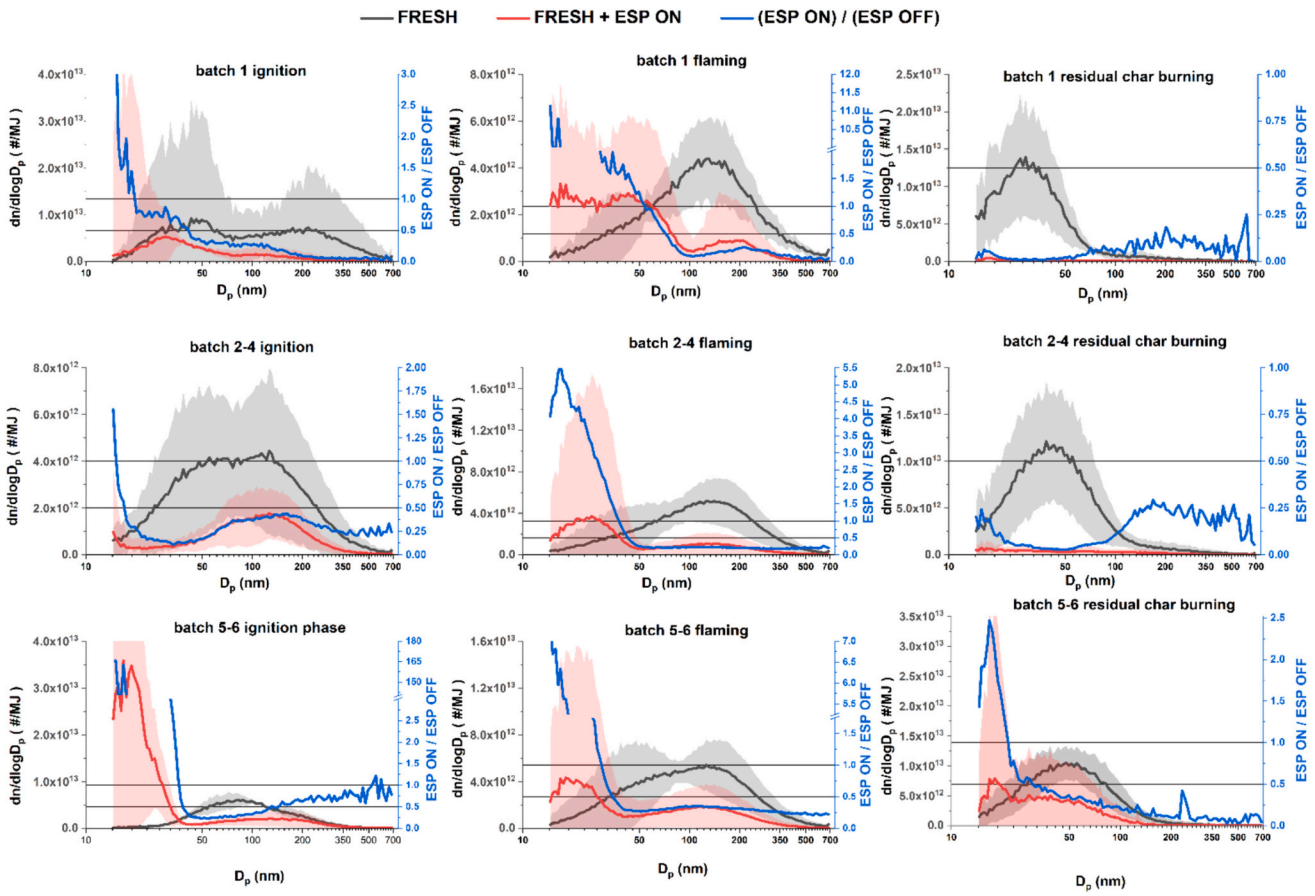

Fig. 3. Fresh particle number size distributions measured by SMPS for different combustion batches and phases without an ESP (black) and with the ESP (red). The ratios of the two number size distributions are shown as blue lines. The distributions are averaged over all experiments, with the shaded areas denoting the standard deviation over the experiments ($n = 3$ for both conditions). The ESP on/ESP off -ratios of 1 (zero reduction efficiency) and 0.5 (reduction efficiency of 50 %) are highlighted as horizontal lines.

The alveolar particle fraction is considered very important for human health effects because particles deposited in the deepest region of human lungs cannot be evicted out naturally, while the alveolar region is also where the particles may pass into blood circulation (Kocbach Bølling et al., 2009; Nakane, 2012). The highest submicron LDSA concentrations were observed during the flaming phase combustion by particles in the 4th and 5th size bin of ELPI in the range of 50–214 nm (Supplementary Fig. S8), which is also the particle size range with largest deposition efficiency in the alveolar region compared to trachea-bronchial and Head airways region (Supplementary Fig. S2). On the other hand, particles larger than 300 nm deposit mainly on the upper respiratory track. The LDSA concentration in HA region was around 30 % of the total, because of the lower number fraction of particles >300 nm compared to sub-100 nm particles in RWC emissions. LDSA deposition into the TB region accounted only 10.5 % of total LDSA deposition, which might partly be a consequence of the instrumental limitation of ELPI (and NSAM) in measuring particles below 20 nm in size, since TB deposition is the most efficient for particles in the size range 1–10 nm according to the ICRP deposition model (Supplementary Fig. S2b).

We estimated that ALV-LDSA EF from ignition, flaming and char burning phases were (2.07 ± 1.09) x10^{11} μm^2/MJ, (2.77 ± 1.32) x10^{11} μm^2/MJ, and (1.42 ± 0.46) x10^{11} μm^2/MJ, respectively, covering 58 %, 59 %, and 64 % of the total LDSA, respectively. This suggests residual char burning emitted particles are slightly more prone to deposit in the ALV region, but overall particle number concentrations of ignition and flaming phases were much higher leading to higher ALV LDSA concentrations for these two phases. The particle mass normalized LDSA values (LDSA/$PM_{0.9}$, Table 1, Fig. 4) indicate the highest ALV-LDSA per unit mass of emission for char burning phase and lowest for ignition phase. This trend was same for mass-normalized TB-LDSA concentrations. For HA region, the highest average LDSA per unit of submicron particulate

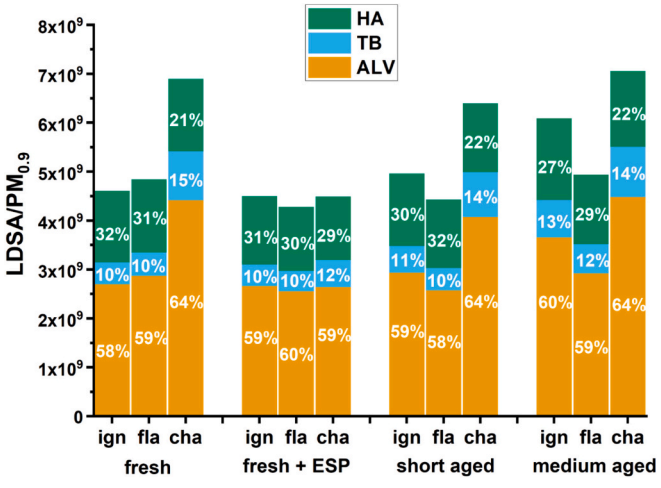

Fig. 4. Average LDSA per unit mass of $PM_{0.9}$ for the different regions of human respiratory track (head airways (HA), tracheobronchial (TB) and alveolar (ALV)) in the different combustion phases(ign = ignition, fla = flaming, cha = residual char burning) as estimated for fresh, fresh with ESP on, short aged and medium aged RWC emissions ($n = 3$ for each). Percentages indicate the fraction of total LDSA in different regions of a respiratory track.

mass was observed for flaming phase and the lowest for ignition phase, although the average HA-LDSA/$PM_{0.9}$ values had little difference among all phases (Table 1, Fig. 4).

The LDSA emissions peaked during stable flaming phase at the middle of individual combustion batches (Fig. 5a; timeseries of the NSAM TB-LDSA are available in Supplementary Fig. S9), simultaneously with the eBC and $PM_{0.9}$ concentrations (Fig. 2c, Supplementary Fig. S10), indicating BC particles as an important contributor to LDSA. The eBC and total LDSA emissions had a strong correlation for fresh RWC emission ($R^2 = 0.86$, Supplementary Fig. S11). The correlation of eBC and LDSA was highest for flaming phase ($R^2 = 0.86$, Supplementary Fig. S12a), when the BC mass fraction in the emitted particulate mass was the highest (Supplementary Fig. S13a). The lower correlation during the ignition phase ($R^2 = 0.63$) was likely caused by the larger contribution of organic matter to the total $PM_{0.9}$ and subsequently the LDSA. As expected for the char burning phase with negligible eBC emissions, there was no correlation between eBC and LDSA ($R^2 = 0.01$). Correlations with the NSAM TB-LDSA and eBC follow similar trends, and are shown in Supplementary Fig. S9. BC particles have previously been shown to be the key constituent of PM that dominates deposition in respiratory track in urban environment (Lepistö et al., 2022). This observation seems to hold for RWC emissions as well, especially from flaming phase combustion.

3.5. Effects of aging on LDSA

The total LDSA concentrations averaged over the whole duration of the experiments were 29 % and 33 % higher in short and medium aged emissions compared to fresh emission, respectively, while average $PM_{0.9}$ emissions were 22 % and 16 % higher, respectively. Thus, the average LDSA concentrations per unit mass also increased (Fig. 4, Supplementary Fig. S13). It should be noted that in addition to impacts of aging, there may also have been differences in the primary emission contents because of the overall repeatability of batchwise combustion of wood. Due to this reason, the LDSA results have been normalized by the $PM_{0.9}$. The increment in LDSA was most prominent for the ignition phase, for which 27 % and 41 % increases in LDSA/$PM_{0.9}$ were measured for short and medium aged emissions (Table 1), respectively, in comparison with fresh emission. The increase can be explained by the gas to particle conversion in the sub-100 nm size range driven by photochemical reactions, leading to new particle formation. LDSA is also impacted by the compaction of the particles (Supplementary Figs. S5 and S6) due to two reasons. Firstly, the densification of particles modifies their inertial deposition characteristics in the respiratory track, especially for the HA (Supplementary Fig. S2c). However, the HA-LDSA didn't notably increase by aging (Table 1), due to the overall small size of the RWC emitted particles (Supplementary Figs. S3-S4). So, in our experiments, densification did not play a significant role in the observed LDSA increase. Secondly, in reality, the compaction of soot agglomerates will lead to decrease in their specific surface area. However, in ELPI-based LDSA estimation particles are considered spherical, thereby neglecting the differences in specific surface areas of agglomerate particles. Overall, the decrease in surface area due to compaction or inertial deposition to HA region plays only a minor role compared to photochemical aging induced new particle formation.

The temporal trends of LDSA concentrations in aged emissions also differed compared to the fresh emissions. For example, while the LDSA of fresh emissions peaked at the middle of individual combustion batches, the long-aged particles exhibited the largest LDSA concentrations at the beginning of every batch (Fig. 5d) with typically high NMVOC emissions (Fig. 2b), which serve as SOA precursors. Consequently, the correlation between the eBC and LDSA was weak for short aged and very weak for medium aged particles ($R^2 = 0.24$ and $R^2 = 0.18$ respectively; Supplementary Fig. S11). This indicates SOA particles were likely the major source of LDSA in aged RWC emissions and that lung-deposition characteristics of aged particles were not dictated by BC particles. There were however clear differences between the phases depending on the VOC emissions. We observed medium correlation between eBC and total LDSA (Supplementary Fig. S12c) for short aged particles during the flaming phase ($R^2 = 0.56$), when soot emissions dominated over secondary aerosol emissions from VOC. After further aging, this correlation became very weak for medium aged even during flaming phase ($R^2 = 0.26$; Supplementary Fig. S12d).

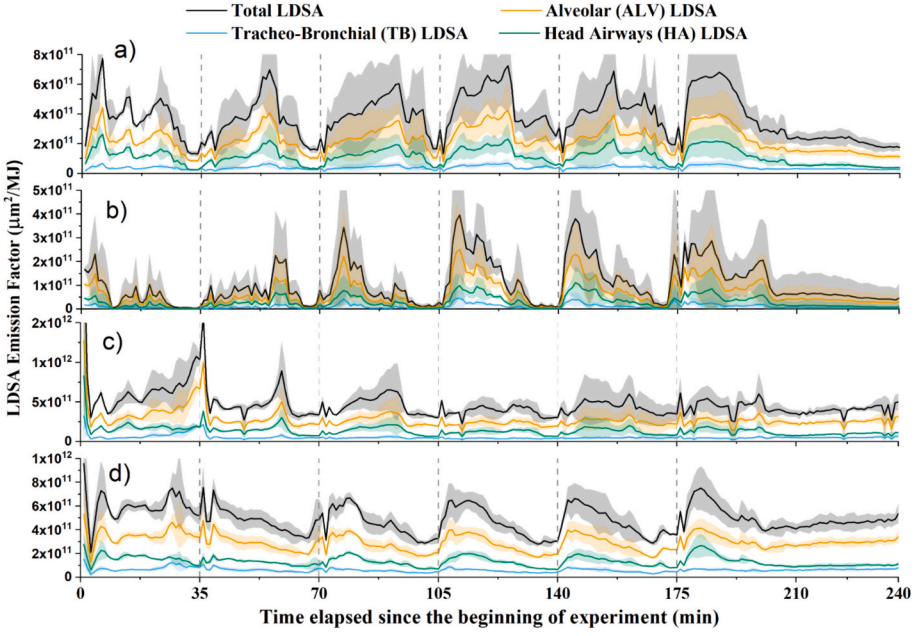

Fig. 5. Timeseries of LDSA emission factors for the different regions of human respiratory track as estimated by ELPI-ICRP model for a) freshly emitted particles, b) fresh emission in presence of ESP, c) short aged particles, and d) medium aged particles. The solid lines represent the average at each timepoint over all experiment days, while the shaded areas represent the standard deviations.

3.6. Effects of electrostatic precipitation on fresh aerosol emissions

The usage of the ESP decreased fine particle mass ($PM_{0.9}$) EFs on average 71 %, which is well in agreement with previous studies on ESP particle reduction efficiency with wood log stoves (Brunner et al., 2018; Oehler and Hartmann, 2014). For eBC and particle number (N_{ELPI}) EFs, the average reduction efficiencies were 69 % and 51 %. In general, the particle removal efficiency of ESP decreased with progressive batches of combustion (Fig. 6). During the first batch the $PM_{0.9}$, eBC, and particle number reduction efficiencies were 85 %, 89 %, and 65 %, respectively. For the 5th and 6th batches of the experiments the average reduction efficiencies for $PM_{0.9}$, eBC, and particle number dropped to 64 %, 67 %, and 46 % respectively. The decrease in reduction efficiency appears to be related to the decrease in the measured ESP power as the experiment progressed (Supplementary Fig. S14). The reduction in power was probably due to elevated flue gas temperature in ESP, which influences the stability of the corona discharge resulting in a decrease in the breakthrough voltage (Suhonen et al., 2021). The ESP control tries to maximize the ESP voltage and a drop in ESP power is related to the automatic ESP function to avoid breakthroughs during operation (Brunner et al., 2018). In addition, slow decline in collection efficiency was observed day to day which was probably caused by soot deposit formation on the electrode and the walls (Brunner et al., 2018).

The comparison of particle size distributions with ESP on and off show that the removal of particles was dependent on combustion phase as well as particle size (Fig. 3). RWC emitted particles can be chemically classified into three components with significantly different electrical conductivities: (i) inorganic salts, (ii) EC, and (iii) condensable organic compounds (Vicente et al., 2022). However, these components can exist both as internally and externally mixed in RWC exhausts (Tissari et al., 2009). The combustion conditions dictate the relative abundance of these three components, with flaming combustion emission primarily being rich in EC-dominated soot and char burning emission dominated by inorganic salts (Kortelainen et al., 2018). For our experiments, the $PM_{0.9}$ and number reduction efficiencies were the highest for the char burning phase (87 % and 68 % respectively), which can be explained by the abundance of inorganic-rich particles. The average $PM_{0.9}$ reduction efficiencies for organic-dominated emissions during ignition phase and soot dominated emission of flaming phase were 74 % and 68 %, respectively (Fig. 6). For N_{ELPI}, the average ESP reduction efficiencies were only 51 % for ignition phase and 57 % for flaming phase. Electrical conductivity of inorganic salts has been found to be ideal for removal by ESP, while the high conductivity of soot may lead to the re-entrainment of agglomerated particles (Nussbaumer and Lauber, 2010). Further, ESP efficiency may also go down simply because of high particulate load during the eBC-rich flaming phase.

Interestingly, the number concentrations of particles smaller than 50 nm, especially sub-30 nm particles, were observed to increase in presence of ESP compared to the fresh emission without ESP during ignition and flaming phases (Fig. 3). On average, an increase of 41 % and 33 % in sub-50 nm N_{ELPI} EF was observed during the ignition and flaming phases, respectively. This observed new particle formation can result from ESP efficiently decreasing particulate condensation sink in the flue gas by the removal of seed particles, thereby promoting nucleation of particles from organic or inorganic vapours (Suhonen et al., 2021). Secondly, the ions and ozone produced by the ESP may also promote oxidation of organic vapours leading to nucleation of new particles (Xiang et al., 2016). The composition of OA in these experiments has been comprehensively studied in a separate study (Schneider et al., 2024), where the use of ESP was indeed found to lead to formation of

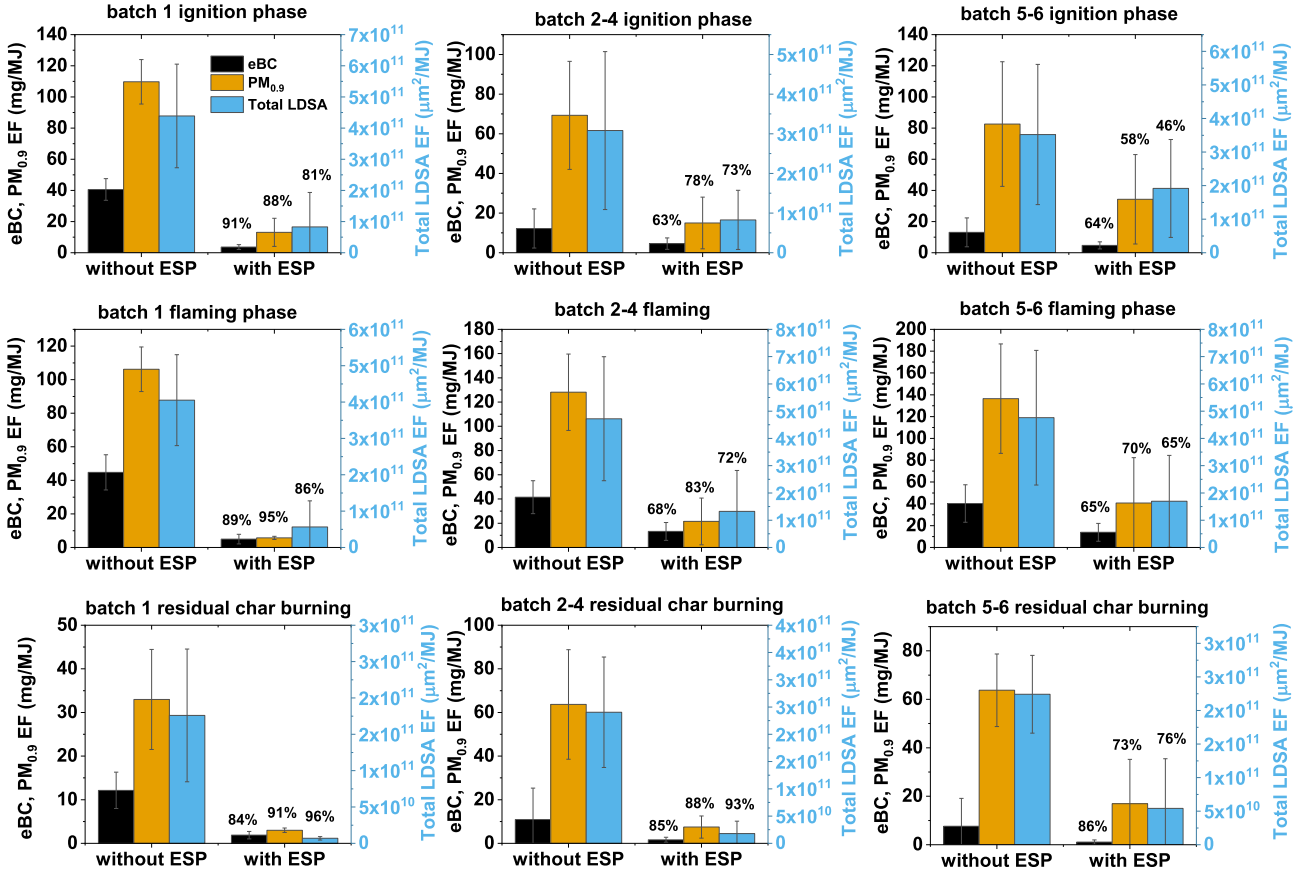

Fig. 6. Reduction efficiency of ESP for eBC, $PM_{0.9}$ and total LDSA concentrations for different combustion batches and phases, averaged over all experiment days for fresh ($n = 3$) and fresh with ESP on ($n = 3$) experiments. Error bar indicates the standard deviation, and the reduction efficiencies are mentioned as numeric values for corresponding parameters.

additional oxygenated compounds. These effects are likely synergic, as any ozone- and ion-induced oxidation of gaseous organic compounds can decrease their vapour pressures, which together with the reduced availability of seed particles will promote new particle formation by nucleation.

The particle densities of fresh RWC emissions were also altered by the variation in reduction efficiencies for different chemical constituents. For particles produced from ignition and flaming phases, there was no significant change in particle densities between the ESP on and off experiments (Supplementary Fig. S5b). For the residual char burning phase, in contrast, the overall density of the remaining particles decreased (Table 1) as the ESP efficiently removed the highly dense ash derived salt particles. As a result of the ESP induced changes in particle number size distribution and effective densities, the overall total LDSA concentrations of fresh RWC seemed to decrease in presence of ESP. The average LDSA emission factors over all three ESP-on experiments were $(6.5 \pm 8.5) \times 10^{10}$ μm^2/MJ, $(1.1 \pm 1.5) \times 10^{10}$ μm^2/MJ and $(3 \pm 3.8) \times 10^{10}$ μm^2/MJ for ALV, TB and HA regions, respectively. Compared to fresh RWC emission, the overall reductions were 72 %, 73 %, and 74 % in ALV-, TB-, and HA-LDSA EFs, respectively. The discrepancy between the NSAM and ELPI-based TB-LDSAs was higher with the ESP on, presumably due to the production of ultrafine particles for which the NSAM is known to have low response (Asbach et al., 2012; Todea et al., 2015).

For the ignition phase and flaming phases, the correlations of eBC and total LDSA were similar with or without the ESP, with the exception that the intercept for the eBC vs LDSA correlation is smaller for the ESP case, and the ratios of LDSA to eBC slightly higher (Supplementary Figs. S11 and S12b). For the residual char burning phase, the total LDSA appeared to have no dependency on eBC, similarly to all other studied cases. The use of the ESP reduced the LDSA/$PM_{0.9}$-ratio of the residual char burning phase, specifically, by efficiently reducing the small inorganic particles and changing the relative deposition fractions (Fig. 4, Supplementary Fig. S13).

4. Conclusions

We estimated combustion phase specific LDSA emission factors of a modern woodstove and explored the relationships between eBC and LDSA in fresh and aged RWC emissions. Further, the impacts of utilizing an electrostatic precipitator in the flue gas stack were assessed for fresh emissions. For fresh RWC emission, flaming combustion-derived total LDSA had the highest correlation with eBC ($R^2 = 0.93$), which is in line with the previous works that have highlighted BC particles to dominate LDSA concentrations in urban and coastal environment. On the other hand, eBC didn't appear to have any contribution to LDSA concentrations from residual char burning emissions. The LDSA concentrations measured by a relatively simple nanoparticle surface area monitor (NSAM) were constantly underestimated in comparison to the ELPI-ICPR method, with higher discrepancy after photochemical aging or with the ESP in use. Nevertheless, the excellent correlations between the two methods applied for the LDSA estimation indicate that the NSAM could be useful for assessing LDSA emissions of wood stoves.

We observed an overall increase in LDSA emission factors due to the simulated photochemical aging, primarily aided by formation of ultrafine nucleated particles. On the other hand, the simultaneous compaction and densification of the agglomerated particles would decrease the LDSA. In total, photochemical aging decreased the eBC dependency of LDSA. The decrease in correlation was most notable for ignition phase, where organic gaseous emissions and consequent secondary aerosol formation were the highest. For the flaming phase, in contrast, a strong correlation between eBC and LDSA remained after short aging, but only moderate correlation was observed after more extensive photochemical aging. This implies that for ambient air monitoring, eBC would work as a proxy for LDSA only in environments governed by fresh combustion emissions.

The use of an ESP reduced the average $PM_{0.9}$, eBC, and total LDSA emission factors by roughly 70 %, but increased the number emissions of sub-30 nm nanoparticles. ESP removed alkali salts produced during residual char burning very efficiently as seen by the reduction in particle effective density specifically for the residual char burning phase. The correlation between LDSA and eBC EFs for flaming phase emission remained good even in presence of the ESP. The reduction efficiencies decreased along consecutive combustion batches as the experiment progressed, most likely caused by increase in flue gas temperature and partly due to the formation of soot deposits in the ESP. Overall, the small ESP was found to be a relatively efficient method for abating fine particulate mass, equivalent black carbon and LDSA emissions from a log wood-fired wood stove. However, the long-term performance of such ESPs and the observed increase in nanoparticle emissions still require further investigation. Further, the effects of EPSs and other wood stove exhaust after-treatment systems on the secondary aerosol pollutant formation need to be studied.

The need to monitor and regulate LDSA on national and higher (e.g., EU) levels calls for thorough characterization of its sources in order to mitigate the health effects of urban air pollution. Residential combustion has been suggested to be an important source of LDSA in urban air (Kuula et al., 2020; Kaskaoutis et al., 2022). The nature of batchwise RWC is very variable, and depends on multiple factors, including stove design, combustion protocol, and fuel characteristics, such as wood species and wood log size and moisture content (Hartikainen et al., 2020; Kortelainen et al., 2018; Rinta-Kiikka et al., 2024; Tissari et al., 2009). In this work, we have thoroughly characterized LDSA emissions of a modern wood stove utilizing combustion air-staging and a relatively optimal user operation of the stove. The results can be utilized to evaluate the role of RWC in ambient LDSA levels and the efficiency of ESP as a method to mitigate RWC-derived air pollution.

CRediT authorship contribution statement

A. Mukherjee: Writing – original draft, Visualization, Methodology, Investigation, Conceptualization. **A. Hartikainen:** Writing – original draft, Visualization, Supervision, Formal analysis. **J. Joutsensaari:** Writing – review & editing, Software, Methodology. **S. Basnet:** Investigation, Formal analysis. **A. Mesceriakovas:** Methodology, Investigation, Formal analysis. **M. Ihalainen:** Methodology, Investigation. **P. Yli-Pirilä:** Methodology, Investigation. **J. Leskinen:** Investigation, Supervision. **M. Somero:** Investigation. **J. Louhisalmi:** Investigation. **Z. Fang:** Formal analysis. **M. Kalberer:** Supervision, Resources, Project administration. **Y. Rudich:** Writing – review & editing, Supervision, Resources, Project administration, Funding acquisition. **J. Tissari:** Writing – review & editing, Investigation. **H. Czech:** Writing – review & editing, Supervision, Investigation. **R. Zimmermann:** Supervision, Resources, Project administration, Funding acquisition, Conceptualization. **O. Sippula:** Writing – original draft, Supervision, Project administration, Investigation, Funding acquisition, Conceptualization.

Declaration of competing interest

The authors declare that they have no known competing financial interests or personal relationships that could have appeared to influence the work reported in this paper.

Data availability

Data will be made available on request.

Acknowledgements

Funding: This work was supported by the Helmholtz Association (HGF) by the Helmholtz International Laboratory aeroHEALTH (InterLabs-0005) and the Helmholtz Virtual Institute of Complex Molecular Systems in Environmental Health - Aerosols and Health (HICE), and the

Research Council of Finland project BBrCAC [grant no. 341597]. A.M acknowledges the EDUFI Fellowship Grant from the Finnish National Agency for Education (TM-21-11567) and the LUMETO Doctoral Fellowship provided by the University of Eastern Finland. M.I. is supported by the Research Council of Finland competitive funding to strengthen university research profiles (PROFI) for the University of Eastern Finland.

Appendix A. Supplementary data

Supplementary data to this article can be found online at https://doi.org/10.1016/j.scitotenv.2024.175840.

References

Alves, C., Gonçalves, C., Fernandes, A.P., Tarelho, L., Pio, C., 2011. Fireplace and woodstove fine particle emissions from combustion of western Mediterranean wood types. Atmos. Res. 101 (3), 692–700. https://doi.org/10.1016/j.atmosres.2011.04.015.

Asbach, C., Fissan, H., Stahlmecke, B., Kuhlbusch, T.A.J., Pui, D.Y.H., 2009. Conceptual limitations and extensions of lung-deposited Nanoparticle Surface Area Monitor (NSAM). J. Nanopart. Res. 11 (1), 101–109. https://doi.org/10.1007/s11051-008-9479-8.

Asbach, C., Kaminski, H., Von Barany, D., Kuhlbusch, T.A.J., Monz, C., Dziurowitz, N., Pelzer, J., Vossen, K., Berlin, K., Dietrich, S., Götz, U., Kiesling, H.J., Schierl, R., Dahmann, D., 2012. Comparability of portable nanoparticle exposure monitors. Ann. Occup. Hyg. 56 (5), 606–621. https://doi.org/10.1093/annhyg/mes033.

Barmet, P., Dommen, J., DeCarlo, P.F., Tritscher, T., Praplan, A.P., Platt, S.M., Prévôt, A.S.H., Donahue, N.M., Baltensperger, U., 2012. OH clock determination by proton transfer reaction mass spectrometry at an environmental chamber. Atmos. Meas. Tech. 5 (3), 647–656. https://doi.org/10.5194/amt-5-647-2012.

Basnet, S., Hartikainen, A., Virkkula, A., Yli-Pirilä, P., Kortelainen, M., Suhonen, H., Kilpeläinen, L., Ihalainen, M., Väätäinen, S., Louhisalmi, J., Somero, M., Tissari, J., Jakobi, G., Zimmermann, R., Kilpeläinen, A., Sippula, O., 2024. Contribution of brown carbon to light absorption in emissions of European residential biomass combustion appliances. Atmos. Chem. Phys. 24 (5), 3197–3215. https://doi.org/10.5194/acp-24-3197-2024.

Bertrand, A., Stefenelli, G., Bruns, E.A., Pieber, S.M., Temime-Roussel, B., Slowik, J.G., Prévôt, A.S.H., Wortham, H., El Haddad, I., Marchand, N., 2017. Primary emissions and secondary aerosol production potential from woodstoves for residential heating: influence of the stove technology and combustion efficiency. Atmos. Environ. 169, 65–79. https://doi.org/10.1016/j.atmosenv.2017.09.005.

Brunner, T., Wuercher, G., Obernberger, I., 2018. 2-year field operation monitoring of electrostatic precipitators for residential wood heating systems. Biomass Bioenergy 111, 278–287. https://doi.org/10.1016/j.biombioe.2017.01.025.

Bruns, E.A., Krapf, M., Orasche, J., Huang, Y., Zimmermann, R., Drinovec, L., Močnik, G., El-Haddad, I., Slowik, J.G., Dommen, J., Baltensperger, U., Prévôt, A.S.H., 2015. Characterization of primary and secondary wood combustion products generated under different burner loads. Atmos. Chem. Phys. 15 (5), 2825–2841. https://doi.org/10.5194/acp-15-2825-2015.

Chakrabarty, R.K., Moosmüller, H., Garro, M.A., Arnott, W.P., Walker, J., Susott, R.A., Babbitt, R.E., Wold, C.E., Lincoln, E.N., Hao, W.M., 2006. Emissions from the laboratory combustion of wildland fuels: particle morphology and size. J. Geophys. Res. Atmos. 111, D07204. https://doi.org/10.1029/2005JD006659.

Charvet, A., Bau, S., Bémer, D., Thomas, D., 2015. On the importance of density in ELPI data post-treatment. Aerosol Sci. Technol. 49 (12), 1263–1270. https://doi.org/10.1080/02786826.2015.1117568.

Chen, J., Li, C., Ristovski, Z., Milic, A., Gu, Y., Islam, M.S., Wang, S., Hao, J., Zhang, H., He, C., Guo, H., Fu, H., Miljevic, B., Morawska, L., Thai, P., LAM, Y.F., Pereira, G., Ding, A., Huang, X., Dumka, U.C., 2017. A review of biomass burning: emissions and impacts on air quality, health and climate in China. Sci. Total Environ. 579, 1000–1034. https://doi.org/10.1016/j.scitotenv.2016.11.025.

Cheristanidis, S., Grivas, G., Chaloulakou, A., 2020. Determination of total and lung-deposited particle surface area concentrations, in central Athens, Greece. Environ. Monit. Assess. 192 (10), 627. https://doi.org/10.1007/s10661-020-08569-8.

Corbin, J.C., Modini, R.L., Gysel-Beer, M., 2023. Mechanisms of soot-aggregate restructuring and compaction. Aerosol Sci. Technol. 57 (2), 89–111. https://doi.org/10.1080/02786826.2022.2137385.

Cornette, J.F.P., Dyakov, I.V., Plissart, P., Bram, S., Blondeau, J., 2024. In-situ evaluation of a commercial electrostatic precipitator integrated in a small-scale wood chip boiler. J. Electrost. 128, 103897 https://doi.org/10.1016/j.elstat.2024.103897.

Czech, H., Sippula, O., Kortelainen, M., Tissari, J., Radischat, C., Passig, J., Streibel, T., Jokiniemi, J., Zimmermann, R., 2016. On-line analysis of organic emissions from residential wood combustion with single-photon ionisation time-of-flight mass spectrometry (SPI-TOFMS). Fuel 177, 334–342. https://doi.org/10.1016/j.fuel.2016.03.036.

Czech, H., Miersch, T., Orasche, J., Abbaszade, G., Sippula, O., Tissari, J., Michalke, B., Schnelle-Kreis, J., Streibel, T., Jokiniemi, J., Zimmermann, R., 2018. Chemical composition and speciation of particulate organic matter from modern residential small-scale wood combustion appliances. Sci. Total Environ. 612, 636–648. https://doi.org/10.1016/j.scitotenv.2017.08.263.

Directive 2009/125/EC of the European Parliament and of the Council of 21 October 2009 establishing a framework for the setting of ecodesign requirements for energy-related product, 2009. European Commission. http://data.europa.eu/eli/dir/2009/125/oj.

Drinovec, L., Močnik, G., Zotter, P., Prévôt, A.S.H., Ruckstuhl, C., Coz, E., Rupakheti, M., Sciare, J., Müller, T., Wiedensohler, A., Hansen, A.D.A., 2015. The dual-spot Aethalometer: an improved measurement of aerosol black carbon with real-time loading compensation. Atmos. Meas. Tech. 8 (5), 1965–1979. https://doi.org/10.5194/amt-8-1965-2015.

Enekwizu, O.Y., Hasani, A., Khalizov, A.F., 2021. Vapor condensation and coating evaporation are both responsible for soot aggregate restructuring. Environ. Sci. Technol. 55 (13), 8622–8630. https://doi.org/10.1021/acs.est.1c02391.

Fierz, M., Houle, C., Steigmeier, P., Burtscher, H., 2011. Design, calibration, and field performance of a miniature diffusion size classifier. Aerosol Sci. Technol. 45 (1), 1–10. https://doi.org/10.1080/02786826.2010.516283.

Fissan, H., Neumann, S., Trampe, A., Pui, D.Y.H., Shin, W.G., 2006. Rationale and principle of an instrument measuring lung deposited nanoparticle surface area. J. Nanopart. Res. 9 (1), 53–59. https://doi.org/10.1007/s11051-006-9156-8.

Gonçalves, C., Alves, C., Pio, C., 2012. Inventory of fine particulate organic compound emissions from residential wood combustion in Portugal. Atmos. Environ. 50, 297–306. https://doi.org/10.1016/j.atmosenv.2011.12.013.

Grahame, T.J., Klemm, R., Schlesinger, R.B., 2014. Public health and components of particulate matter: the changing assessment of black carbon. J. Air Waste Manage. Assoc. 64 (6), 620–660. https://doi.org/10.1080/10962247.2014.912692.

Guarnieri, M., Balmes, J.R., 2014. Outdoor air pollution and asthma. Lancet 383 (9928), 1581–1592. https://doi.org/10.1016/S0140-6736(14)60617-6.

Hama, S.M.L., Ma, N., Cordell, R.L., Kos, G.P.A., Wiedensohler, A., Monks, P.S., 2017. Lung deposited surface area in Leicester urban background site/UK: sources and contribution of new particle formation. Atmos. Environ. 151, 94–107. https://doi.org/10.1016/j.atmosenv.2016.12.002.

Hartikainen, A., Tiitta, P., Ihalainen, M., Yli-Pirilä, P., Orasche, J., Czech, H., Kortelainen, M., Lamberg, H., Suhonen, H., Koponen, H., Hao, L., Zimmermann, R., Jokiniemi, J., Tissari, J., Sippula, O., 2020. Photochemical transformation of residential wood combustion emissions: dependence of organic aerosol composition on OH exposure. Atmos. Chem. Phys. 20 (11), 6357–6378. https://doi.org/10.5194/acp-20-6357-2020.

Helin, A., Niemi, J.V., Virkkula, A., Pirjola, L., Teinilä, K., Backman, J., Aurela, M., Saarikoski, S., Rönkkö, T., Asmi, E., Timonen, H., 2018. Characteristics and source apportionment of black carbon in the Helsinki metropolitan area, Finland. Atmos. Environ. 190, 87–98. https://doi.org/10.1016/j.atmosenv.2018.07.022.

Hinds, W.C., 1999. Aerosol Technology, Properties, Behaviour, and Measurement of Airborne Particles. John Wiley & Sons Inc, New York.

ICRP, 1994. Human Respiratory Tract Model for Radiological Protection. ICRP Publication 66. Ann. ICRP 24, 1–3.

Ihalainen, M., Tiitta, P., Czech, H., Yli-Pirilä, P., Hartikainen, A., Kortelainen, M., Tissari, J., Stengel, B., Sklorz, M., Suhonen, H., Lamberg, H., Leskinen, A., Kiendler-Scharr, A., Harndorf, H., Zimmermann, R., Jokiniemi, J., Sippula, O., 2019. A novel high-volume Photochemical Emission Aging flow tube Reactor (PEAR). Aerosol Sci. Technol. 53 (3), 276–294. https://doi.org/10.1080/02786826.2018.1559918.

Ihantola, T., Di Bucchianico, S., Happo, M., Ihalainen, M., Uski, O., Bauer, S., Kuuspalo, K., Sippula, O., Tissari, J., Oeder, S., Hartikainen, A., Rönkkö, T.J., Martikainen, M.-V., Huttunen, K., Vartiainen, P., Suhonen, H., Kortelainen, M., Lamberg, H., Leskinen, A., Jalava, P.I., 2020. Influence of wood species on toxicity of log-wood stove combustion aerosols: a parallel animal and air-liquid interface cell exposure study on spruce and pine smoke. Part. Fibre Toxicol. 17 (1), 27. https://doi.org/10.1186/s12989-020-00355-1.

Intergovernmental Panel on Climate Change (Ed.), 2014. Climate Change 2013 – The Physical Science Basis. Cambridge University Press. https://doi.org/10.1017/CBO9781107415324.

Janssen, N.A.H., Hoek, G., Simic-Lawson, M., Fischer, P., van Bree, L., ten Brink, H., Keuken, M., Atkinson, R.W., Anderson, H.R., Brunekreef, B., Cassee, F.R., 2011. Black carbon as an additional Indicator of the adverse health effects of airborne particles compared with PM_{10} and $PM_{2.5}$. Environ. Health Perspect. 119 (12), 1691–1699. https://doi.org/10.1289/ehp.1003369.

Jaworek, A., Sobczyk, A.T., Marchewicz, A., Krupa, A., Czech, T., 2021. Particulate matter emission control from small residential boilers after biomass combustion. A review. Renew. Sust. Energ. Rev. 137, 110446 https://doi.org/10.1016/j.rser.2020.110446.

Kaskaoutis, D.G., Grivas, G., Oikonomou, K., Tavernaraki, P., Papoutsidaki, K., Tsagkaraki, M., Stavroulas, I., Zarmpas, P., Paraskevopoulou, D., Bougiatioti, A., Liakakou, E., Gavrouzou, M., Dumka, U.C., Hatzianastassiou, N., Sciare, J., Gerasopoulos, E., Mihalopoulos, N., 2022. Impacts of severe residential wood burning on atmospheric processing, water-soluble organic aerosol and light absorption, in an inland city of Southeastern Europe. Atmos. Environ. 280 https://doi.org/10.1016/j.atmosenv.2022.119139.

Keller, A., Burtscher, H., 2017. Characterizing particulate emissions from wood burning appliances including secondary organic aerosol formation potential. J. Aerosol Sci. 114, 21–30. https://doi.org/10.1016/j.jaerosci.2017.08.014.

Klauser, F., Carlon, E., Kistler, M., Schmidl, C., Schwabl, M., Sturmlechner, R., Haslinger, W., Kasper-Giebl, A., 2018. Emission characterization of modern wood stoves under real-life oriented operating conditions. Atmos. Environ. 192, 257–266. https://doi.org/10.1016/j.atmosenv.2018.08.024.

Kocbach Bølling, A., Pagels, J., Yttri, K.E., Barregard, L., Sallsten, G., Schwarze, P.E., Boman, C., 2009. Health effects of residential wood smoke particles: the importance of combustion conditions and physicochemical particle properties. Part. Fibre Toxicol. 6 (1), 29. https://doi.org/10.1186/1743-8977-6-29.

Kortelainen, M., Jokiniemi, J., Tiitta, P., Tissari, J., Lamberg, H., Leskinen, J., Grigonyte-Lopez Rodriguez, J., Koponen, H., Antikainen, S., Nuutinen, I., Zimmermann, R., Sippula, O., 2018. Time-resolved chemical composition of small-scale batch combustion emissions from various wood species. Fuel 233, 224–236. https://doi.org/10.1016/j.fuel.2018.06.056.

Koullapis, P.G., Stylianou, F.S., Sznitman, J., Olsson, B., Kassinos, S.C., 2020. Towards whole-lung simulations of aerosol deposition: A model of the deep lung. J. Aerosol Sci. 144, 105541 https://doi.org/10.1016/j.jaerosci.2020.105541.

Kukkonen, J., López-Aparicio, S., Segersson, D., Geels, C., Kangas, L., Kauhaniemi, M., Maragkidou, A., Jensen, A., Assmuth, T., Karppinen, A., Sofiev, M., Hellén, H., Riikonen, K., Nikmo, J., Kousa, A., Niemi, J.V., Karvosenoja, N., Sousa Santos, G., Sundvor, I., Brandt, J., 2020. The influence of residential wood combustion on the concentrations of PM2.5 in four Nordic cities. Atmos. Chem. Phys. 20 (7), 4333–4365. https://doi.org/10.5194/acp-20-4333-2020.

Kumar, P., Robins, A., Vardoulakis, S., Britter, R., 2010. A review of the characteristics of nanoparticles in the urban atmosphere and the prospects for developing regulatory controls. Atmos. Environ. 44 (39), 5035–5052. https://doi.org/10.1016/j.atmosenv.2010.08.016.

Kuula, J., Kuuluvainen, H., Niemi, J.V., Saukko, E., Portin, H., Kousa, A., Aurela, M., Rönkkö, T., Timonen, H., 2020. Long-term sensor measurements of lung deposited surface area of particulate matter emitted from local vehicular and residential wood combustion sources. Aerosol Sci. Technol. 54 (2), 190–202. https://doi.org/10.1080/02786826.2019.1668909.

Kuuluvainen, H., Rönkkö, T., Järvinen, A., Saari, S., Karjalainen, P., Lähde, T., Pirjola, L., Niemi, J.V., Hillamo, R., Keskinen, J., 2016. Lung deposited surface area size distributions of particulate matter in different urban areas. Atmos. Environ. 136, 105–113. https://doi.org/10.1016/j.atmosenv.2016.04.019.

Lamberg, H., Sippula, O., Joutsensaari, J., Ihalainen, M., Tissari, J., Lähde, A., Jokiniemi, J., 2018. Analysis of high-temperature oxidation of wood combustion particles using tandem-DMA technique. Combust. Flame 191, 76–85. https://doi.org/10.1016/j.combustflame.2017.12.027.

Lelieveld, J., Evans, J.S., Fnais, M., Giannadaki, D., Pozzer, A., 2015. The contribution of outdoor air pollution sources to premature mortality on a global scale. Nature 525 (7569), 367–371. https://doi.org/10.1038/nature15371.

Lepistö, T., Kuuluvainen, H., Juuti, P., Järvinen, A., Arffman, A., Rönkkö, T., 2020. Measurement of the human respiratory tract deposited surface area of particles with an electrical low pressure impactor. Aerosol Sci. Technol. 54 (8), 958–971. https://doi.org/10.1080/02786826.2020.1745141.

Lepistö, T., Kuuluvainen, H., Lintusaari, H., Kuittinen, N., Salo, L., Helin, A., Niemi, J.V., Manninen, H.E., Timonen, H., Jalava, P., Saarikoski, S., Rönkkö, T., 2022. Connection between lung deposited surface area (LDSA) and black carbon (BC) concentrations in road traffic and harbour environments. Atmos. Environ. 272, 118931 https://doi.org/10.1016/j.atmosenv.2021.118931.

Leskinen, J., Ihalainen, M., Torvela, T., Kortelainen, M., Lamberg, H., Tiitta, P., Jakobi, G., Grigonyte, J., Joutsensaari, J., Sippula, O., Tissari, J., Virtanen, A., Zimmermann, R., Jokiniemi, J., 2014. Effective density and morphology of particles emitted from small-scale combustion of various wood fuels. Environ. Sci. Technol. 48 (22), 13298–13306. https://doi.org/10.1021/es502214a.

Leskinen, J., Hartikainen, A., Väätäinen, S., Ihalainen, M., Virkkula, A., Mesceriakovas, A., Tiitta, P., Miettinen, M., Lamberg, H., Czech, H., Yli-Pirilä, P., Tissari, J., Jakobi, G., Zimmermann, R., Sippula, O., 2023. Photochemical aging induces changes in the effective densities, morphologies, and optical properties of combustion aerosol particles. Environ. Sci. Technol. 57 (13), 5137–5148. https://doi.org/10.1021/acs.est.2c04151.

Liu, X., Hadiatullah, H., Zhang, X., Trechera, P., Savadkoohi, M., Garcia-Marlès, M., Reche, C., Pérez, N., Beddows, D.C.S., Salma, I., Thén, W., Kalkavouras, P., Mihalopoulos, N., Hueglin, C., Green, D.C., Tremper, A.H., Chazeau, B., Gille, G., Marchand, N., Querol, X., 2023. Ambient air particulate total lung deposited surface area (LDSA) levels in urban Europe. Sci. Total Environ. 898, 165466 https://doi.org/10.1016/j.scitotenv.2023.165466.

Löndahl, J., Massling, A., Swietlicki, E., Vaclavik Bräuner, E., Ketzel, M., Pagels, J., Loft, S., 2009. Experimentally determined human respiratory tract deposition of airborne particles at a busy street. Environ. Sci. Technol. 43 (13), 4659–4664. https://doi.org/10.1021/es803029b.

Michelsen, H.A., Colket, M.B., Bengtsson, P.-E., D'Anna, A., Desgroux, P., Haynes, B.S., Miller, J.H., Nathan, G.J., Pitsch, H., Wang, H., 2020. A review of terminology used to describe soot formation and evolution under combustion and pyrolytic conditions. ACS Nano 14 (10), 12470–12490. https://doi.org/10.1021/acsnano.0c06226.

Miersch, T., Czech, H., Hartikainen, A., Ihalainen, M., Orasche, J., Abbaszade, G., Tissari, J., Streibel, T., Jokiniemi, J., Sippula, O., Zimmermann, R., 2019. Impact of photochemical ageing on Polycyclic Aromatic Hydrocarbons (PAH) and oxygenated PAH (Oxy-PAH/OH-PAH) in logwood stove emissions. Sci. Total Environ. 686, 382–392. https://doi.org/10.1016/j.scitotenv.2019.05.412.

Moreno-Ríos, A.L., Tejeda-Benítez, L.P., Bustillo-Lecompte, C.F., 2022. Sources, characteristics, toxicity, and control of ultrafine particles: an overview. Geosci. Front. 13 (1) https://doi.org/10.1016/j.gsf.2021.101147.

Mylläri, F., Pirjola, L., Lihavainen, H., Asmi, E., Saukko, E., Laurila, T., Vakkari, V., O'Connor, E., Rautiainen, J., Häyrinen, A., Niemelä, V., Maunula, J., Hillamo, R., Keskinen, J., Rönkkö, T., 2019. Characteristics of particle emissions and their atmospheric dilution during co-combustion of coal and wood pellets in a large combined heat and power plant. J. Air Waste Manage. Assoc. 69 (1), 97–108. https://doi.org/10.1080/10962247.2018.1521349.

Nakane, H., 2012. Translocation of particles deposited in the respiratory system: a systematic review and statistical analysis. Environ. Health Prev. Med. 17 (4), 263–274. https://doi.org/10.1007/s12199-011-0252-8.

Ni, M., Huang, J., Lu, S., Li, X., Yan, J., Cen, K., 2014. A review on black carbon emissions, worldwide and in China. Chemosphere 107, 83–93. https://doi.org/10.1016/j.chemosphere.2014.02.052.

Nicolaou, L., Fandiño-Del-Rio, M., Koehler, K., Checkley, W., 2021. Size distribution and lung-deposited doses of particulate matter from household exposure to biomass smoke. Indoor Air 31 (1), 51–62. https://doi.org/10.1111/ina.12710.

Ntziachristos, L., Polidori, A., Phuleria, H., Geller, M.D., Sioutas, C., 2007. Application of a diffusion charger for the measurement of particle surface concentration in different environments. Aerosol Sci. Technol. 41 (6), 571–580. https://doi.org/10.1080/02786820701272020.

Nussbaumer, T., Lauber, A., 2010. Formation mechanism and physical properties of particles from wood combustion for design and operation of electrostatic precipitators. In: 18th European Biomass Conference and Exhibition, 113, pp. 3–7.

Oberdörster, G., Oberdörster, E., Oberdörster, J., 2005. Nanotoxicology: an emerging discipline evolving from studies of ultrafine particles. Environ. Health Perspect. 113 (7), 823–839. https://doi.org/10.1289/ehp.7339.

Oehler, H., Hartmann, H., 2014. Comparative long-term field and test stand measurements at small scale electrostatic precipitators-experiences and measurement strategies. In: 22nd European Biomass Conference and Exhibition, pp. 381–387. https://doi.org/10.5071/22ndEUBCE2014-2AO.1.4.

Olfert, J., Rogak, S., 2019. Universal relations between soot effective density and primary particle size for common combustion sources. Aerosol Sci. Technol. 53 (5), 485–492. https://doi.org/10.1080/02786826.2019.1577949.

Omara, M., Hopke, P.K., Raja, S., Holsen, T.M., 2010. Performance evaluation of a model electrostatic precipitator for an advanced wood combustion system. Energy Fuel 24 (12), 6301–6306. https://doi.org/10.1021/ef101031u.

Ortega, R., Bresson, C., Darolles, C., Gautier, C., Roudeau, S., Perrin, L., Janin, M., Floriani, M., Aloin, V., Carmona, A., Malard, V., 2014. Low-solubility particles and a Trojan-horse type mechanism of toxicity: the case of cobalt oxide on human lung cells. Part. Fibre Toxicol. 11 (1), 14. https://doi.org/10.1186/1743-8977-11-14.

Peng, Z., Jimenez, J.L., 2020. Radical chemistry in oxidation flow reactors for atmospheric chemistry research. Chem. Soc. Rev. 49 (9), 2570–2616. https://doi.org/10.1039/C9CS00766K.

Pokhrel, R.P., Gordon, J., Fiddler, M.N., Bililign, S., 2021. Impact of combustion conditions on physical and morphological properties of biomass burning aerosol. Aerosol Sci. Technol. 55 (1), 80–91. https://doi.org/10.1080/02786826.2020.1822512.

Reche, C., Viana, M., Brines, M., Pérez, N., Beddows, D., Alastuey, A., Querol, X., 2015. Determinants of aerosol lung-deposited surface area variation in an urban environment. Sci. Total Environ. 517, 38–47. https://doi.org/10.1016/j.scitotenv.2015.02.049.

Reda, A.A., Czech, H., Schnelle-Kreis, J., Sippula, O., Orasche, J., Weggler, B., Abbaszade, G., Arteaga-Salas, J.M., Kortelainen, M., Tissari, J., Jokiniemi, J., Streibel, T., Zimmermann, R., 2015. Analysis of gas-phase carbonyl compounds in emissions from modern wood combustion appliances: influence of wood type and combustion appliance. Energy Fuel 29 (6), 3897–3907. https://doi.org/10.1021/ef502877c.

Rinta-Kiikka, H., Dahal, K., Louhisalmi, J., Koponen, H., Sippula, O., Krpec, K., Tissari, J., 2024. The effect of wood species on fine particle and gaseous emissions from a modern wood stove. Atmosphere 15 (7), 839. https://doi.org/10.3390/atmos15070839.

Rissler, J., Messing, M.E., Malik, A.I., Nilsson, P.T., Nordin, E.Z., Bohgard, M., Sanati, M., Pagels, J.H., 2013. Effective density characterization of soot agglomerates from various sources and comparison to aggregation theory. Aerosol Sci. Technol. 47 (7), 792–805. https://doi.org/10.1080/02786826.2013.791381.

Salo, L., Rönkkö, T., Saarikoski, S., Teinilä, K., Kuula, J., Alanen, J., Arffman, A., Timonen, H., Keskinen, J., 2021. Concentrations and size distributions of particle Lung-deposited Surface Area (LDSA) in an underground mine. Aerosol Air Qual. Res. 21 (8), 200660 https://doi.org/10.4209/aaqr.200660.

Savolahti, M., Karvosenoja, N., Soimakallio, S., Kupiainen, K., Tissari, J., Paunu, V.-V., 2019a. Near-term climate impacts of Finnish residential wood combustion. Energy Policy 133, 110837. https://doi.org/10.1016/j.enpol.2019.06.045.

Savolahti, M., Lehtomäki, H., Karvosenoja, N., Paunu, V.-V., Korhonen, A., Kukkonen, J., Kupiainen, K., Kangas, L., Karppinen, A., Hänninen, O., 2019b. Residential wood combustion in Finland: PM2.5 emissions and health impacts with and without abatement measures. Int. J. Environ. Res. Public Health 16 (16), 2920. https://doi.org/10.3390/ijerph16162920.

Schmid, O., Stoeger, T., 2016. Surface area is the biologically most effective dose metric for acute nanoparticle toxicity in the lung. J. Aerosol Sci. 99, 133–143. https://doi.org/10.1016/j.jaerosci.2015.12.006.

Schneider, E., Czech, H., Hartikainen, A., Hansen, H.J., Gawlitta, N., Ihalainen, M., Yli-Pirilä, P., Somero, M., Kortelainen, M., Louhisalmi, J., Orasche, J., Fang, Z., Rudich, Y., Sippula, O., Rüger, C.P., Zimmermann, R., 2024. Molecular composition of fresh and aged aerosols from residential wood combustion and gasoline car with modern emission mitigation technology. Environ Sci Process Impacts 26, 1295–1309. https://doi.org/10.1039/D4EM00106K.

Shin, W.G., Pui, D.Y.H., Fissan, H., Neumann, S., Trampe, A., 2007. Calibration and numerical simulation of nanoparticle surface area monitor (TSI Model 3550 NSAM). J. Nanopart. Res. 9 (1), 61–69. https://doi.org/10.1007/s11051-006-9153-y.

Sippula, O., Hytönen, K., Tissari, J., Raunemaa, T., Jokiniemi, J., 2007. Effect of wood fuel on the emissions from a top-feed pellet stove. Energy Fuel 21 (2), 1151–1160. https://doi.org/10.1021/ef060286e.

Stockwell, C.E., Yokelson, R.J., Kreidenweis, S.M., Robinson, A.L., DeMott, P.J., Sullivan, R.C., Reardon, J., Ryan, K.C., Griffith, D.W.T., Stevens, L., 2014. Trace gas emissions from combustion of peat, crop residue, domestic biofuels, grasses, and other fuels: configuration and Fourier transform infrared (FTIR) component of the

fourth Fire Lab at Missoula Experiment (FLAME-4). Atmos. Chem. Phys. 14 (18), 9727–9754. https://doi.org/10.5194/acp-14-9727-2014.

Suhonen, H., Laitinen, A., Kortelainen, M., Koponen, H., Kinnunen, N., Suvanto, M., Tissari, J., Sippula, O., 2021. Novel fine particle reduction method for wood stoves based on high-temperature electric collection of naturally charged soot particles. J. Clean. Prod. 312, 127831 https://doi.org/10.1016/j.jclepro.2021.127831.

Tebert, Christian, Lisa, Rödig, Ingo, Hartmann, Tobias, Ulbricht, Volker, Lenz, 2020. Umweltzeichen Blauer Engel: Entwicklung von Vergabekriterien für Kaminöfen für Holz. Federal Environment Agency.

Tiitta, P., Leskinen, A., Hao, L., Yli-Pirilä, P., Kortelainen, M., Grigonyte, J., Tissari, J., Lamberg, H., Hartikainen, A., Kuuspalo, K., Kortelainen, A.-M., Virtanen, A., Lehtinen, K.E.J., Komppula, M., Pieber, S., Prévôt, A.S.H., Onasch, T.B., Worsnop, D. R., Czech, H., Sippula, O., 2016. Transformation of logwood combustion emissions in a smog chamber: formation of secondary organic aerosol and changes in the primary organic aerosol upon daytime and nighttime aging. Atmos. Chem. Phys. 16 (20), 13251–13269. https://doi.org/10.5194/acp-16-13251-2016.

Tissari, J., Lyyränen, J., Hytönen, K., Sippula, O., Tapper, U., Frey, A., Saarnio, K., Pennanen, A.S., Hillamo, R., Salonen, R.O., Hirvonen, M.-R., Jokiniemi, J., 2008. Fine particle and gaseous emissions from normal and smouldering wood combustion in a conventional masonry heater. Atmos. Environ. 42 (34), 7862–7873. https://doi.org/10.1016/j.atmosenv.2008.07.019.

Tissari, J., Hytönen, K., Sippula, O., Jokiniemi, J., 2009. The effects of operating conditions on emissions from masonry heaters and sauna stoves. Biomass Bioenergy 33 (3), 513–520. https://doi.org/10.1016/j.biombioe.2008.08.009.

Todea, A.M., Beckmann, S., Kaminski, H., Asbach, C., 2015. Accuracy of electrical aerosol sensors measuring lung deposited surface area concentrations. J. Aerosol Sci. 89, 96–109. https://doi.org/10.1016/j.jaerosci.2015.07.003.

Todea, A.M., Beckmann, S., Kaminski, H., Bard, D., Bau, S., Clavaguera, S., Dahmann, D., Dozol, H., Dziurowitz, N., Elihn, K., Fierz, M., Lidén, G., Meyer-Plath, A., Monz, C., Neumann, V., Pelzer, J., Simonow, B.K., Thali, P., Tuinman, I., Asbach, C., 2017. Inter-comparison of personal monitors for nanoparticles exposure at workplaces and in the environment. Sci. Total Environ. 605–606, 929–945. https://doi.org/10.1016/j.scitotenv.2017.06.041.

Torvela, T., Tissari, J., Sippula, O., Kaivosoja, T., Leskinen, J., Virén, A., Lähde, A., Jokiniemi, J., 2014. Effect of wood combustion conditions on the morphology of freshly emitted fine particles. Atmos. Environ. 87, 65–76. https://doi.org/10.1016/j.atmosenv.2014.01.028.

Vicente, E.D., Alves, C.A., Martins, V., Almeida, S.M., Lazaridis, M., 2021. Lung-deposited dose of particulate matter from residential exposure to smoke from wood burning. Environ. Sci. Pollut. Res. 28 (46), 65385–65398. https://doi.org/10.1007/s11356-021-15215-4.

Vicente, E.D., Duarte, M.A., Tarelho, L.A.C., Alves, C.A., 2022. Efficiency of emission reduction Technologies for Residential Biomass Combustion Appliances: electrostatic precipitator and catalyst. Energies 15 (11), 4066. https://doi.org/10.3390/en15114066.

World Health Organization, 2021. WHO Global Air Quality Guidelines. Particulate Matter (PM2.5 and PM10), Ozone, Nitrogen Dioxide, Sulfur Dioxide and Carbon Monoxide. WHO European Centre for Environment and Health.

Wu, Y., Xia, Y., Huang, R., Deng, Z., Tian, P., Xia, X., Zhang, R., 2019. A study of the morphology and effective density of externally mixed black carbon aerosols in ambient air using a size-resolved single-particle soot photometer (SP2). Atmos. Meas. Tech. 12 (8), 4347–4359. https://doi.org/10.5194/amt-12-4347-2019.

Xiang, J., Weschler, C., J., Mo, J., Day, D., Zhang, J., Zhang, Y., 2016. Ozone, electrostatic precipitators, and particle number concentrations: correlations observed in a real office during working hours. Environ. Sci. Technol. 50 (18), 10236–10244. https://doi.org/10.1021/acs.est.6b03069.

Yokelson, R.J., Susott, R., Ward, D.E., Reardon, J., Griffith, D.W.T., 1997. Emissions from smoldering combustion of biomass measured by open-path Fourier transform infrared spectroscopy. J. Geophys. Res. Atmos. 102 (D15), 18865–18877. https://doi.org/10.1029/97JD00852.

Yus-Díez, J., Bernardoni, V., Močnik, G., Alastuey, A., Ciniglia, D., Ivančič, M., Querol, X., Perez, N., Reche, C., Rigler, M., Vecchi, R., Valentini, S., Pandolfi, M., 2021. Determination of the multiple-scattering correction factor and its cross-sensitivity to scattering and wavelength dependence for different AE33 Aethalometer filter tapes: a multi-instrumental approach. Atmos. Meas. Tech. 14 (10), 6335–6355. https://doi.org/10.5194/amt-14-6335-2021.